The Journal of Experimental Biology 209, 1516-1534
Published by The Company of Biologists 2006
doi:10.1242/jeb.02154

Median fin function in bluegill sunfish *Lepomis macrochirus*: streamwise vortex structure during steady swimming

Eric D. Tytell

Department of Organismic and Evolutionary Biology, Harvard University, Cambridge, MA 02138, USA

Present address: Department of Biology, University of Maryland, College Park, MD 20742, USA (e-mail: tytell@post.harvard.edu)

Accepted 7 February 2006

Summary

Fishes have an enormous diversity of body shapes and fin morphologies. From a hydrodynamic standpoint, the functional significance of this diversity is poorly understood, largely because the three-dimensional flow around swimming fish is almost completely unknown. Fully three-dimensional volumetric flow measurements are not currently feasible, but measurements in multiple transverse planes along the body can illuminate many of the important flow features. In this study, I analyze flow in the transverse plane at a range of positions around bluegill sunfish *Lepomis macrochirus*, from the trailing edges of the dorsal and anal fins to the near wake. Simultaneous particle image velocimetry and kinematic measurements were performed during swimming at 1.2 body lengths s^{-1} to describe the streamwise vortex structure, to quantify the contributions of each fin to the vortex wake, and to assess the importance of three-dimensional flow effects in swimming.

Sunfish produce streamwise vortices from at least eight distinct places, including both the dorsal and ventral margins of the soft dorsal and anal fins, and the tips and central notched region of the caudal fin. I propose a three-dimensional structure of the vortex wake in which these vortices from the caudal notch are elongated by the dorso-ventral cupping motion of the tail, producing a structure like a hairpin vortex in the caudal fin vortex ring. Vortices from the dorsal and anal fin persist into the wake, probably linking up with the caudal fin vortices. These dorsal and anal fin vortices do not differ significantly in circulation from the two caudal fin tip vortices. Because the circulations are equal and the length of the trailing edge of the caudal fin is approximately equal to the combined trailing edge length of the dorsal and anal fins, I argue that the two anterior median fins produce a total force that is comparable to that of the caudal fin. To provide additional detail on how different positions contribute to total force along the posterior body, the change in vortex circulation as flow passes down the body is also analyzed. The posterior half of the caudal fin and the dorsal and anal fins add vortex circulation to the flow, but circulation appears to decrease around the peduncle and anterior caudal fin. Kinematic measurements indicate that the tail is angled correctly to enhance thrust through this interaction. Finally, the degree to which the caudal fin acts like a idealized two-dimensional plate is examined: approximately 25% of the flow near the tail is accelerated up and down, rather than laterally, producing wasted momentum, a loss not present in ideal two-dimensional theories.

Key words: fluid dynamics, streamwise vortex, particle image velocimetry, median fin, dorsal fin, anal fin, vortex wake, body shape, bluegill sunfish, *Lepomis macrochirus*.

Introduction

Fish are not two-dimensional. However, swimming fish move primarily in the horizontal plane, undulating from side to side as they propel themselves forward. The apparent two-dimensional (2D) character of the motion has led both hydrodynamic and kinematic studies of fish swimming to focus on a 2D slice through the horizontal midline (e.g. Breder, 1926; Carling et al., 1998; Lighthill, 1960; Lindsey, 1978; Müller et al., 1997; Tytell and Lauder, 2004; Weihs, 1972; Wu, 1971). This approach has allowed researchers to make headway in understanding fish swimming despite the complexity of the fluid dynamics, which has only recently become amenable to detailed experimental measurements (with the development of methods for observing planar flow fields; Willert and Gharib, 1991) and computational simulation.

Even though this approach has been quite successful, it is becoming more apparent that neither the swimming motion nor the flow around the body are 2D. For example, even fish with symmetrical (homocercal) tails, such as bluegill sunfish *Lepomis macrochirus* and chub mackerel *Scomber japonicus*, do not move them symmetrically (Gibb et al., 1999; Lauder, 2000); instead, both fishes angle the dorsal edge of the fin into

the tail motion, leading the ventral lobe through the tail beat cycle. Sunfish and other fishes also cup the dorsal and ventral edges of the caudal fin into the flow (Bainbridge, 1963; Lauder, 2000; Webb, 1975), a clearly three-dimensional (3D) motion. Many fishes also angle their bodies to maintain lift for horizontal swimming (Ferry and Lauder, 1996; He and Wardle, 1986; Liao and Lauder, 2000), showing the importance of fluid dynamic effects perpendicular to the horizontal midline.

Second, several recent hydrodynamic studies have either directly observed 3D effects or inferred their importance. Sharks' asymmetrical tails produce a large vortex ring with a smaller ring inside it produced by the upper lobe (Wilga and Lauder, 2004). A more subtle effect from 3D body shape was described in eels (Tytell and Lauder, 2004). Beginning with the observation (Müller et al., 2001; Tytell and Lauder, 2004) that eels produce a different wake from previously studied fishes, like sunfish or mackerel *Scomber japonicus*, they argued that differences in 2D swimming kinematics were not sufficient to explain the hydrodynamic differences. Instead, they proposed that the more important factor was the different body shapes among the fishes (Lauder and Tytell, 2006).

Third, a 3D computational simulation of swimming fishes found that the flow around a giant danio *Danio aequipinnatus*, which has a generalized teleost morphology, could not be approximated by classical 2D models (Zhu et al., 2002). They simulated motion strictly in the horizontal plane, using an approximation of the giant danio's morphology, but found that this produced a combination of flow down the body and transversely around the body. This combination of flow directions invalidates the assumption of 2D flow in two classic theoretical models (Lighthill, 1971; Wu, 1971).

Three-dimensional body shape may also have subtle effects on swimming efficiency. Three-dimensional airplane wings, for example, lose efficiency because of effects at their tips. As the wings grow shorter relative to their chord (i.e. their aspect ratio grows smaller), these losses become greater (Barnard and Philpott, 1995). For example, Dong et al. simulated flapping wings with varying aspect ratios (Dong et al., 2005). In their simulations, a 2D flapping wing, which does not have tip losses, has a peak propulsive efficiency of greater than 25%, while a 3D wing with a low aspect ratio (2.55; close to that of a bluegill tail, which is around 2.25) has a maximum efficiency of about 20%. At the peak efficiencies, the 2D wing also produces about twice the thrust of the 3D wing (Dong et al., 2005). The performance of the simulated wings is less impressive (Dong et al., 2005) than some other reports for flapping propulsors (e.g. Barrett et al., 1999 report propulsive efficiencies above 90%), but their study provides the only systematic examination of tip losses in flapping propulsion. Regardless of the exact magnitude, fish tails certainly suffer tip losses like the simulated wings due to their 3D shape. Fishes such as tunas, with high-aspect ratio lunate tails, may mitigate these effects, but even for them, the 'cost of three-dimensionality' will never be zero and may be substantial (Dong et al., 2005).

Finally, and more broadly, it is in the third dimension that the diversity of fish body shapes, fin shapes and locations, and swimming modes become important for function. The focus on the horizontal midline, while useful for deriving general principles, cannot explain much of the evolution and adaptation of this diversity. The dorsal and anal fins, for example, move in a complex, active way, different from the body (Standen and Lauder, 2005), and generate their own wakes (Lauder et al., 2002), changing the flow that the caudal fin encounters and possibly enhancing its thrust (Akhtar and Mittal, 2005; Wolfgang et al., 1999; Zhu et al., 2002). To begin to approach the question of the adaptive significance of fish morphology, one must examine 3D fluid flow.

Instantaneous 3D fluid flow measurements around swimming fish are not yet feasible, however (but for a promising technique, see Pereira and Gharib, 2002). Instead, 2D measurements of flow in the transverse plane at multiple positions down the body can illuminate many of the salient features of the 3D flow field. In particular, vortices aligned approximately along the swimming or 'streamwise' direction (termed 'tip vortices' in the aerodynamics literature) are shed nearly constantly by the dorsal and ventral margins of the median fins, but have never been described for a swimming fish. The strength of these vortices relates directly to the overall force and its distribution among fins, and also to efficiency, because much of the energy used to produce them is not useful for thrust.

Therefore, I examine the transverse flow around swimming bluegill sunfish using particle image velocimetry (PIV) in the transverse plane. Flow in multiple planes along the body is described, resulting in the first description of the streamwise vortex pattern around a swimming fish. Putting together the pattern described here with previous data from the horizontal and vertical planes, I propose a new form of the 3D vortex structure around a swimming sunfish. The average relative forces produced by each fin are approximated from the circulation of their vortices, indicating that the dorsal and anal fins together produce a force that is comparable to that produced by the caudal fin.

Materials and methods

Fish

Bluegill sunfish *Lepomis macrochirus* Rafinesque were collected using nets in ponds near Concord, MA, USA. *L. macrochirus* was chosen because both 3D swimming kinematics and flow patterns have been studied in this species (Drucker and Lauder, 1999; Drucker and Lauder, 2000; Drucker and Lauder, 2001; Lauder, 2000; Standen and Lauder, 2005). Animals were maintained at room temperature (~20°C) in separate 40 l freshwater aquaria with a 12 h:12 h photoperiod, and were fed earthworms three times weekly. Four fish of similar size (total body length L=18.3±0.2 cm, mean ± s.e.m.; range 17.7–18.7 cm) were selected for wake visualization experiments.

Swimming protocol and flow visualization

Sunfish swam individually in the center of the working area (28 cm×28 cm×80 cm) of a variable-speed freshwater flow tank. Steady swimming was elicited at $1.20\,L\,s^{-1}$ (approximately $22\,cm\,s^{-1}$), slightly faster than the gait transition speed in which sunfish begin using their caudal fins together with the pectoral fins (Drucker and Lauder, 2000). Animals were gently maneuvered into the center of the working section using a wooden dowel, which was removed before filming a swimming sequence. Swimming sequences were collected so that the light sheet illuminated six approximate positions along the body: the trailing edge of the soft dorsal and anal fins, the caudal peduncle, the base, middle and trailing edge of the caudal fin, and the wake just posterior to the caudal fin. Wake sequences were carefully chosen so that the tail did not intersect the light sheet, but was still partially visible through it to allow the fish's location to be determined. Far wake measurements were not made, due to the difficulty of determining the fish's position precisely without being able to view it in the PIV images.

Fluid flow in the transverse plane was filmed using two high speed digital cameras, a configuration that enabled use of the stereo PIV algorithm (Gaydon et al., 1997; Prasad, 2000; Willert, 1997) to correct the strong parallax effect from flow passing through the plane. The cameras viewed the swimming fish from behind through a 12.7 cm×15.2 cm front-surface mirror placed at 45° in the flow (Fig. 1A). One camera, a Photron APX (Photron USA, Inc., San Diego, CA, USA) with 1024×1024 pixel resolution, was placed so that it viewed the transverse plane orthogonally through a 135 mm lens at a distance of approximately 1.5 m. The other, a Photron FastCam with 1280×1024 pixel resolution, was placed 12° off axis, and used a 50 mm lens at a distance of about 0.72 m (Fig. 1A). The off-axis camera used a Scheimpflüg lens mount (LaVision, Inc., Ypsilanti, MI, USA) to focus on the entire plane, even though it was at an angle to the camera sensor (see Nauen and Lauder, 2002b; Prasad, 2000 for a more detailed description of the optical configuration). The two cameras imaged an overlapping region approximately 12 cm×12 cm in area. An additional Photron FastCam was used to film the silhouette of the fish from below (Fig. 1B) for simultaneous kinematic analysis.

The distance between the mirror and the light sheet was more than twice the mirror's presented width, making effects from the mirror's bow wake negligible in the light sheet plane. Additionally, the presented area of the mirror was 137 cm^2, providing a constriction ratio of 1.2, which should not affect the mean flow velocities substantially. This type of mirror

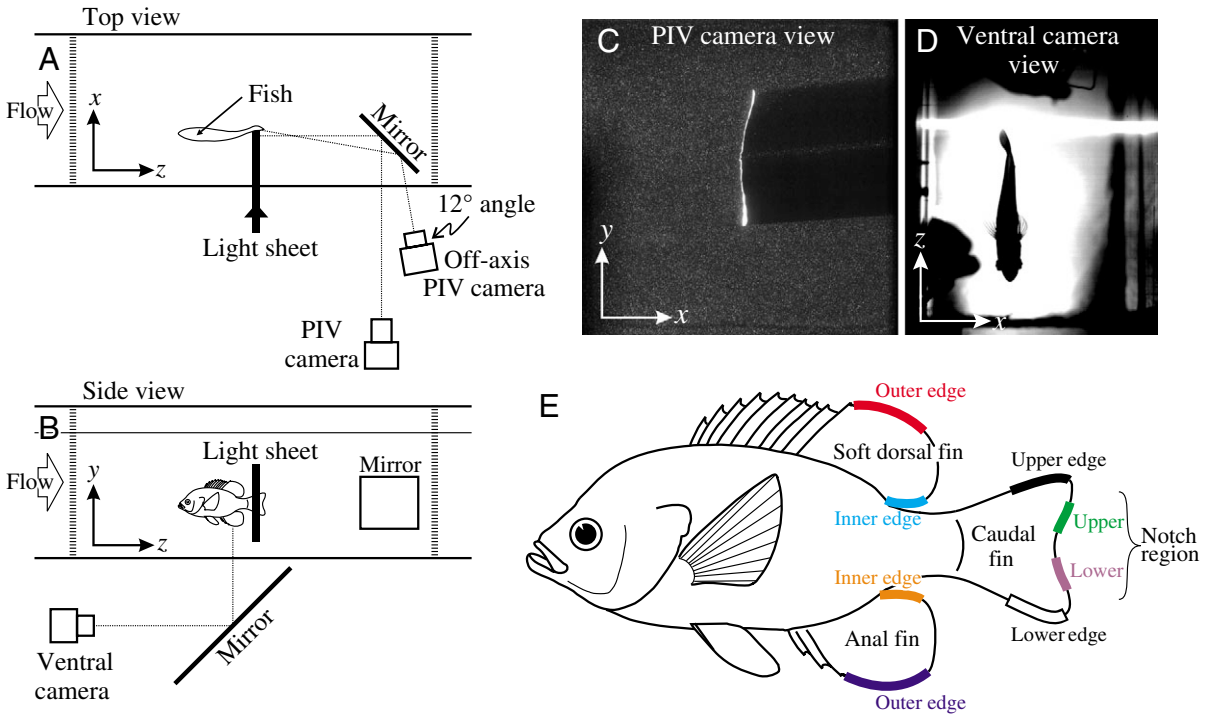

Fig. 1. Filming arrangement. (A) Flow tank filming configuration seen from above. Two cameras film the fish from behind through a front-surface mirror at 45° in the flow downstream of the fish. The mirror, fish, and camera positions are approximately to scale relative to the flow tank width. A laser light sheet is projected in from the side. One camera views the sheet orthogonally; the other is at a 12° angle. The off-axis camera uses a Scheimpflüg lens mount to tilt the axis of the lens and focus on the entire light sheet, despite the camera's angle. The *x* axis is lateral, from the fish's left to right, and the *z* axis is streamwise in the flow direction. (B) Side view of the filming configuration, showing the ventral view camera used for kinematic measurements. PIV cameras are omitted. The *y* axis is dorso-ventral and the *z* axis is streamwise. (C) Sample image from the orthogonal PIV view. (D) Sample image from the ventral view. (E) Terminology for regions in which streamwise vortices are shed. Sources of vortices along the body are indicated by thick colored lines.

configuration has been used previously and has been shown not to affect swimming kinematics (Ferry and Lauder, 1996).

A 10 W argon-ion laser was used to project a 3 mm thick light sheet through the side of the tank, illuminating near-neutrally buoyant 12 μm diameter silver-coated glass beads (density 1.3 g cm^{-3}; Potter Industries, Valley Forge, PA, USA). Particle motion was analyzed using a stereo digital particle image velocimetry (PIV) algorithm (Gaydon et al., 1997; Prasad, 2000; Willert, 1997). Camera calibration, the stereo PIV algorithm, and initial vector post-processing were performed using DaVis 7.0.9 (LaVision, Ypsilanti, MI, USA). Cameras were calibrated for each experimental procedure using a grid of crosses with 8 mm×8 mm spacing placed at three different streamwise positions separated by 3 mm each. Cross displacements were fitted using a pinhole camera model (Hartley and Zissermann, 2000). Fitted parameters included the calibration grid position and angle relative to the camera sensor, camera focal length, first and second order radial distortion, principal point and pixel squareness. A self-calibration procedure (Wieneke, 2005) was performed on particle images from steady flow to adjust the fitted light sheet position and angle. The PIV algorithm used three passes, starting with a grid size of 32×32 pixels (approximately 4 mm×4 mm) overlapping by 25% and stepping down to 12×12 pixels (1.5 mm×1.5 mm) overlapping by 50%. A second order correlation for error correction (Hart, 2000) was used in the first two passes. The flow field was initially assumed to have the nominal through-plane flow velocity. After processing, vectors were eliminated if the signal-to-noise ratio was less than 2, and by an iterative procedure that used the median and RMS velocities in a 3×3 vector neighborhood (similar to Nogueira et al., 1997). Finally, a 3×3 spatial smoothing filter was applied, followed by a 25 Hz low-pass finite impulse response temporal filter. The final vector fields had approximately 155×160 vectors.

To assess maximal in-plane error, simulations of particle motion analyzed using the 2D PIV algorithm were compared to measured flow characteristics from steady flow analyzed using the stereo PIV algorithm with post-processing and all filters. Uniform and vortex motions were simulated. Simulations probably produce overestimates of the error, because the stereo PIV algorithm, as implemented in DaVis 7.0, uses the additional information from the second camera to reduce the overall error. Maximum error in uniform flow was less than 3 mm s^{-1}. Vorticity errors tended to be large (~30%) for vorticity greater than 50 s^{-1} (which was near the maximum observed), probably due both to high shear and inaccuracy of numerical derivatives. In contrast, circulation was accurately estimated to within less than 10% for all but the weakest vortices. Peak locking, the tendency of PIV to produce integer pixel displacements, caused overestimates of 30% or more for vortices with circulations of less than 300 mm^2 s^{-1}. Stereo analysis of steady flow showed that maximum turbulence intensity (the standard deviation of flow velocity; Tennekes and Lumley, 1972) was less than 7 mm s^{-1}, in-plane Reynolds stress (Tennekes and Lumley, 1972) was less than 4 mN m^2, and the standard deviation of background vorticity was less than 5 s^{-1}.

The stereo algorithm was used to correct parallax, which it does implicitly when estimating 3D vectors. Geometrical constraints of the setup did not allow a large enough angle between the two cameras to reconstruct the through-plane velocity component w with sufficient precision to detect the effect of the swimming fish over the mean flow velocity. Error on the through-plane velocity component is proportional to $1/\tan(\theta)$, where θ is the angle between the two cameras (12° in this case) (Prasad, 2000); after smoothing the flow velocities, variation in w was typically on the order of 25–50%. The additive effect of the swimming fish, in contrast, is expected to have a maximum downstream magnitude of less than 20% of the mean flow velocity (Drucker and Lauder, 2001), lower than the measurement error. Nonetheless, the dual-camera setup was necessary to remove parallax effects, which were substantial (typically around 2 cm s^{-1} at the edges of the field) in a single-camera configuration.

Kinematic analysis

Silhouettes of the fish were filmed from a ventral view through a front-surface mirror at a 45° angle using a Photron FastCam high-speed digital video camera with 1280×1024 pixel resolution, synchronized with the two used for flow visualization (Fig. 1B). Midline kinematics were digitized from the silhouettes using custom Matlab 6.5.1 (MathWorks, Natick, MA, USA) routines. The algorithms were modified only slightly from those previously described (Tytell and Lauder, 2004), where they are explained in more detail. Briefly, the head and tail positions were digitized manually to provide starting coordinates for a procedure that used one-dimensional cross-correlation to find dark regions with the known width of the fish body. Midlines were then smoothed simultaneously along the body and through time using a 2D smoothing spline (Matlab spaps routine) to produce a mean squared error of approximately 0.25 $pixel^2$ (a 2D analog of the method recommended by Walker, 1998). Once the midline was determined, the position of the maximum lateral excursion at each point on the body was tracked to determine the body amplitude, frequency, wave speed and wave length. Changes in the algorithms from the procedure used by Tytell and Lauder (Tytell and Lauder, 2004) were primarily to avoid errors in the region illuminated by the laser. The digitized midlines were then used to determine the distance of the head from the light sheet, running along the curve of the body, to estimate precisely the laser position relative to the fish.

The dorso-ventral position of the fish in the light sheet was determined from the PIV images. The dorsal and ventral edges of the body were manually digitized. Successive planes were aligned by matching the digitized dorso-ventral positions to the lateral profile of the body, based on a lateral image of one of the experimental individuals during swimming. Additionally, the outline of the body and fins in the transverse images was manually digitized, primarily for visualization

purposes, but also for a simple kinematic analysis of fin curvature and for identification of near-body flow. Five points were identified along the body or caudal fin (upper and lower margins, center, and two additional points to approximate the curvature of the upper and lower lobes). If the dorsal or anal fins were visible, five points were also digitized along each. Spline-based interpolation was used to produce a smooth outline.

Vortex analysis

The circulation and geometry of vortex loops has been used previously to estimate forces on swimming animals (e.g. Drucker and Lauder, 1999; Müller et al., 1997; Nauen and Lauder, 2002a; Tytell, 2004). In this approximation, average force is proportional to the area circumscribed by a vortex loop and the circulation Γ of the vortex, where circulation is defined as:

$$\Gamma = \oint \mathbf{u}.\mathbf{t} ds \,, \quad (1)$$

integrating around a loop enclosing the vortex, where **u** is the fluid velocity vector, **t** is a unit vector tangent to the contour, and s is arc length along the contour. Strictly, force is proportional to circulation only in steady flow, not the complex unsteady motion of swimming fish (Dabiri, 2005), but previous studies (e.g. Drucker and Lauder, 1999; Spedding et al., 2003; Warrick et al., 2005) have found agreement between this approximation and other force measurements.

The goal of the vortex analysis in this study was to assess the relative contributions of different fins to time-averaged overall force and to examine at what points along the body forces are produced. For these purposes, the circulation produced at different locations along the body is a sufficiently accurate approximation of force production. No effort was made to examine every possible source of vorticity, which would be necessary for an accurate estimate of total force (Spedding et al., 2003), nor were assessments made of any unsteady effects (Dabiri, 2005). Because of the uncertainties introduced by this method of analysis, I did not make direct estimates of force; instead, I examined only circulation and use it to make order of magnitude arguments about force.

An additional source of complexity in the analysis is the identification of vortices. In fact, the precise definition of a vortex is currently debated in the fluid dynamics community (see, e.g., Haller, 2005). The intuitive definition of a vortex as a region with rotating flow, for example, is dependent on the choice of reference frame. The vorticity is also not useful in unambiguously identifying vortices, because it is present in shear layers, regions that are clearly not 'vortices', in the intuitive sense. A better metric (Adrian et al., 2000; Vollmers, 2001), though not the only one, for defining a vortex is the swirling strength, or discriminant for complex eigenvalues:

$$(\partial u/\partial x + \partial v/\partial y)^2 - 4(\partial u/\partial x \partial v/\partial y - \partial u/\partial y \partial v/\partial x) \,, \quad (2)$$

where u and v are the horizontal (lateral) and vertical (dorso-ventral) components of fluid velocity, and x and y are the corresponding positions (Fig. 1). The swirling strength is large and negative in regions that are rotating more than shearing or diverging (Vollmers, 2001). Note that swirling strength does not depend on the direction of the rotation. It does not capture every instance that could be called a vortex, nor is it consistent in every reference frame (Haller, 2005), but it does help automate the search for rotating regions of fluid.

Because this study involved a large number of PIV data frames (approximately 4800), a simple automatic procedure was developed for detecting and tracking vortices. The goal of this procedure was not strict hydrodynamic consistency, but rather a rapid identification of the vortices that would have been found by a manual method (as used in all previous studies of swimming hydrodynamics, including Müller et al., 2001; Nauen and Lauder, 2002a; Tytell, 2004). A custom Matlab program found connected regions with large negative values of the swirling strength below a threshold λ. Connected regions below the threshold were identified using a standard image segmentation routine (Matlab's bwlabeln function) in three dimensions (two spatial dimensions and time) with 18 neighbor connectivity (for more information on image segmentation, see Gonzalez et al., 2003). Circulation was estimated for each region by generating an ellipse in each frame that enclosed the thresholded area, interpolating the fluid velocity on to the ellipse using a cubic spline, and numerically evaluating Eqn 1 using a trapezoidal approximation (Matlab's trapz function; Press et al., 1992). Two additional criteria were imposed to eliminate noise or small turbulent eddies: (1), connected regions were required to persist over a minimum time τ, and (2), were required to reach a minimum circulation Γ_{min} in at least one frame.

The parameters λ, τ and Γ_{min} were tuned manually for each swimming bout until the main vortices (those shed by the outer edges of the dorsal and anal fins and by the upper and lower edges of the caudal fin) were consistently detected. Values of λ were 200 or 300 s^{-2}; τ was 12% of a tail beat cycle; and Γ_{min} was 200 or 300 $mm^2\ s^{-1}$, the minimum circulation that could be measured accurately. Detected vortices were manually deleted when they overlapped the images of the fish's body or the shadow region.

All vortices produced by this analysis will be termed 'detected'. Of these vortices, some were clearly formed at specific points along the fish's body, and will thus be termed 'identified'; others could not be definitively assigned to a specific source, and will be called 'unidentified'. Both the circulation magnitude and positions of the identified vortices were fairly insensitive to the choice of λ, τ and Γ_{min}.

The terminology used for vortex shedding regions along the body is shown in Fig. 1E, based on that in Jenkins and Burkhead (Jenkins and Burkhead, 1994). Streamwise vortices are shed from the soft dorsal fin along its dorsal margin (termed 'outer edge') and along the free ventral margin ('inner edge'). Equivalently, from the anal fin, vortices are shed from the ventral margin ('outer edge') and the free dorsal margin ('inner edge'). Note that the inner edges of both fins are distinct from the bases of the fins, where the fin rays insert on to the body. The dorsal and anal fin together will be referred to as the anterior median fins, to distinguish them from the caudal fin.

Streamwise vortices from the caudal fin are shed at its dorsal and ventral margins, termed 'upper' and 'lower', respectively. The terms 'dorsal' and 'ventral' are avoided for the caudal fin, to avoid confusion with the dorsal fin itself. Vortices are also shed along the inclined edges of the notch in the fin, which will be termed the 'upper' and 'lower' edges of the 'caudal notch'. Because bluegill sunfish have an emarginate tail, not a forked tail, this region is not called the fork (Jenkins and Burkhead, 1994).

Added circulation

As flow moves down the body, total vortex circulation should increase, both by addition of new vortices and by changes in individual vortex strength. The circulation added at a given point on the body is proportional to the lateral or vertical force applied to the fluid there. To estimate additional circulation, however, one must remove the contribution of circulation that convects into the plane from upstream. This removal requires taking the derivative of circulation with respect to position, following a fluid element as it moves with the flow. Because of the noise in the data, a continuous empirical model was regressed on the circulation magnitude of each vortex. These models were then summed, smoothed to remove discrete jumps when a new vortex was identified, and differentiated.

To define the regression model, first note that circulation is periodic over a tail beat. Because the vortex moves with the local flow speed (which is quite close to the global mean flow speed; Lauder and Tytell, 2006), the peak circulation in this periodic function progresses down the body over time (i.e. the periodic function has a phase shift linearly proportional to the location along the body). For simplicity, a coordinate system that moves with the global mean flow was chosen. The validity of this assumption is tested in the Results section below. In this coordinate system, circulation could be approximated by a model that is linear in its parameters, simplifying the fitting procedure.

The coordinate system is defined as follows. Relative to the flow, position along the body increases at a rate Ut, where U is the flow speed and t is time. If the tail tip has a phase ϕ when a fluid element passes the tip, then a phase α can be defined as the tail's phase when the element started at position s:

$$\alpha = \frac{2\pi(L-s)}{UT} + \phi \,, \tag{3}$$

where L is the length of the fish and T is the tail beat period.

To examine the vortex strength, circulation was fit using a sinusoidal oscillation with an amplitude that changes linearly along the body,

$$\Gamma \sim (a_0+a_1 s)\sin\alpha + (b_0+b_1 s)\cos\alpha + C \,, \tag{4}$$

where a_i and b_i are the fitted coefficients and C is an offset, which is included for completeness, but which should be equal to zero. Higher order polynomial terms and Fourier modes were also tested, using a general model,

$$\Gamma \sim \sum_{j=1}^{m}\sum_{i=0}^{n} a_{ij}s^i \sin j\alpha + \sum_{j=1}^{m}\sum_{i=0}^{n} b_{ij}s^i \cos j\alpha + C \,, \tag{5}$$

where n is the amplitude polynomial order and m is the number of Fourier modes included. The appropriate number of polynomial terms and Fourier modes was determined by examining the change in r^2 of the models as terms were added.

This model is linear in its parameters and was therefore fitted using the multivariate regression function (regress) in the Matlab Statistics Toolbox 4.1. Each vortex's circulation was modeled only over the range of positions in which it was observed, without extrapolating further.

Several other equations were tested, but Eqn 5 proved to have the best combination of simplicity, explanatory power, and ease of fitting. A somewhat better model, mathematically, would be one with a constant phase shift in the sine terms, which would allow the cosine terms to be dropped. Simplifying this equation results in the same one as Eqn 5, but with a nonlinear restriction on a_{ij} and b_{ij} (a_{ij}/b_{ij} is constant for all values of i), which requires a nonlinear fitting algorithm. Unfortunately, the nonlinear fit did not converge well.

Without the above constraint, the general model in Eqn 5 can produce nonlinear changes in circulation amplitude and phase along the body, due to the different weights on the sine and cosine terms. Specifically, the overall amplitude of each Fourier mode is:

$$\left[\left(\sum_i a_{ij}s^i\right)^2 + \left(\sum_i b_{ij}s^i\right)^2\right]^{1/2}, \tag{6}$$

and the phase is:

$$\tan^{-1}\left(\sum_i b_{ij}s^i \Big/ \sum_i a_{ij}s^i\right). \tag{7}$$

The absolute values of the circulations from the separate models for each identified vortex were summed to produce a model of the total circulation magnitude. To avoid discrete jumps at positions where a vortex was first detected, the sum was smoothed slightly using a Gaussian filter. The smoothing makes physical sense, because streamwise vortices probably grow in strength gradually along the edges of the fins, much as tip vortices grow along the length of a highly swept airplane wing (Barnard and Philpott, 1995). The smoothed total circulation was then differentiated along s to estimate the circulation added to the fluid at each point along the body.

Comparison to 2D ideal flow

To examine the influence of effects from 3D flow relative to the ideal 2D case, the amount of flow accelerated in a single coherent direction (mostly laterally) was compared to the amount pushed up and down towards the dorsal and ventral edges. A simple geometric representation E of how effectively the fish avoids producing flows that cancel comes from the

length of the mean velocity vector, close to the body, relative to the mean of all velocity vector lengths:

$$E = \frac{\langle u\rangle^2 + \langle v\rangle^2}{\langle u^2+v^2\rangle}\,, \tag{8}$$

where u and v are the horizontal and vertical components of fluid velocity close to the tail and $\langle\ \rangle$ denotes a mean. E is the fraction of flow close to the body that is going in the same direction. For example, an ideal 2D plate moving laterally would push all of the fluid laterally (vertical flow does not exist, so v is defined to be 0, and $\langle u^2+v^2\rangle=\langle u^2\rangle$) and would therefore have an E of 1. In contrast, a 3D plate pushes some flow laterally and some up and down (any individual v is non-zero, but $\langle v^2\rangle$ is small because up and down motion averages to zero) and thus has $E<1$. The momentum from the vertical flows cancels out, and thus they are wasted for the purposes of producing thrust or lateral forces. This is not to infer that all vertical flows cancel out for a swimming fish, but the momentum that does cancel is not useful for steady swimming. The mean was taken over a line parallel to the body at a distance of twice the average spacing of PIV vectors from the surface.

The metric E is related to the added streamwise circulation, as estimated above, because the vertical flows will form tip vortices when they reach the dorsal and ventral edges. In principle, a more physical representation of the losses the fish incurs due to its 3D shape would therefore be based on the added circulation. However, E was used because of its simplicity, both for calculating and for understanding it.

Statistics

Midline kinematics were compared among individuals using single-factor analysis of variance (ANOVA) on each parameter individually, with individual as a random effect (Milliken and Johnson, 1992). Additionally, tail beat amplitudes at the center of the tail and the upper and lower margins were compared using a two-factor mixed model ANOVA, with a fixed effect of position and a random effect of individual. The same test was performed for the outer and inner edges of the anterior median fins.

The peak circulations of all vortices were compared using a two-factor mixed-model ANOVA, excluding those vortices whose sources could not be identified. The fixed effect in the model was the vortex source, while the random effect was the individual fish. In all mixed-model ANOVAs, care was taken to use the correct denominator in testing for each effect, taking into account the unbalanced data set (for a discussion of unbalanced mixed-model ANOVAs, see Milliken and Johnson, 1992). *Post hoc* pairwise comparisons were performed using Tukey's honestly significant difference (Milliken and Johnson, 1992).

Means are reported with standard errors and numbers of measurements, where appropriate. All ANOVAs were performed using JMP 5.1 (SAS Institute, Cary, NC, USA), while regressions were performed in Matlab.

Results

Steady swimming sequences were gathered along the body at positions from 0.68L to 1.06L. Fish often pitched head downwards or rolled towards the laser light, an unnatural posture probably due to the highly asymmetric visual stimulus from the laser light. Care was taken to analyze sequences in which pitch and roll were minimal, but some amount of each was unavoidable.

At least four steady tail beats at each position were recorded, resulting in 102 total tail beats. One individual did not swim steadily at the most anterior position. Fig. 2 shows the number of tail beats for each individual at each position. Fish typically drifted forward and backward during a sequence by less than 3 mm and never drifted more than 1 cm. Stride length was 0.0061±0.0004L.

Kinematics

Swimming speeds determined from PIV analysis ranged from 1.09 to 1.20 L s^{-1} (mean 1.16±0.03 L s^{-1}). At this speed, fish used both their pectoral fins and caudal fins for propulsion. Caudal fin beat frequency was 2.41±0.02 Hz with a total amplitude (distance between maximum lateral tail tip excursion on each side) of 0.114±0.002L. Body wave speed was 1.90±0.02 L s^{-1}, with a body wave length of 73.2±0.7% of the body. Strouhal number was 0.290±0.004. Individuals varied significantly in all kinematic variables (one-way random-effects ANOVA; $P<0.001$ in all cases except for wave speed, in which $P=0.042$). The kinematic variables above could be estimated twice per tail beat (when the tail reached maximum excursion on either side) and so the number of data points for these estimates was 204.

The fins appeared in the laser light sheet as bright lines (Fig. 1C), allowing an estimation of the dorso-ventral curvature of the trailing edges of the caudal, dorsal, and anal fins. Fig. 3 shows representative tracings of the three fins from one half tail

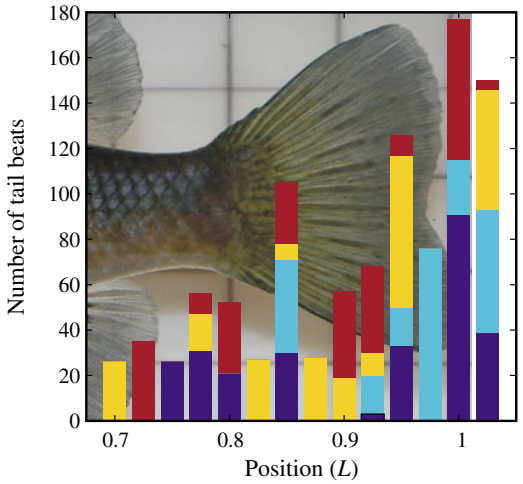

Fig. 2. Number of tail beats collected at different positions along the fish body (L) for four individuals. Individuals are shown as different colors. An image of a fish is shown in the background, scaled appropriately.

beat. Beat frequency was 4.9±0.3 Hz, and did not differ among fins ($F_{6,291}$=0.32; P=0.926). The dorsal and anal fins tended to reach maximum lateral excursion 42% of a period earlier than the caudal fin. The caudal fin curved both upper and lower edges into the flow, with the tips showing a distinct cupping motion, separate from the motion of the center (Fig. 3C). Over the same time period, the upper and lower tips of the caudal fin traversed a distance of 0.118±0.004L and 0.108±0.003L, respectively (22 and 20 mm for L=183 mm, the mean total length) while the center moved 0.070±0.002L (12.9 mm). The ANOVA showed a significant difference among the three positions ($F_{2,6.13}$=12.39; P=0.007) in 49 tail beats near the tail tip, and *post hoc* tests using Tukey's honestly significant difference at a significance level of 0.05 showed that upper and lower tip amplitudes were not significantly different, but they were both different from the center. Individuals showed no evidence of significant variation ($F_{3,6.00}$=3.26; P=0.101). Additionally, the upper and lower tips did not appear to differ in phase from each other, but they both usually led the center by about 9% of the tail beat cycle (as Fig. 3 shows). Comparing excursions for dorsal and anal fin inner and outer edges showed a significant difference among positions ($F_{3,6.22}$=7.32; P=0.019) for 18 tail beats near the fins. *Post hoc* tests at a level of 0.05 indicated that dorsal and anal fins' outer edges moved the same distance, 0.057±0.003L (10.5 mm), but the anal fin's inner edge moved significantly less than the outer edge, 0.041±0.002L (7.6 mm). The dorsal fin inner edge, in contrast, covered the same distance as the outer edge. Individuals showed significant variation ($F_{3,6.01}$=20.46; P=0.002).

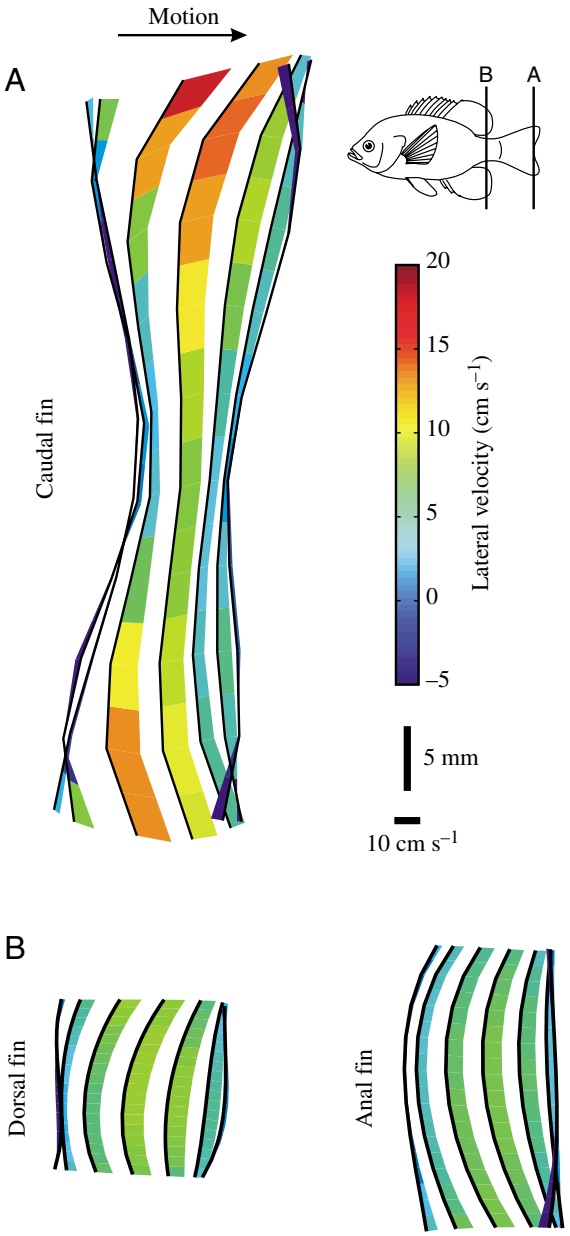

Fig. 3. Tips of the caudal, dorsal and anal fins cup actively into the flow. Motion of fins through half a tail beat from left to right in two transverse planes is presented. Each panel shows 7 tracings of the posterior margins of the fins, spaced equally in time, as seen from behind the fish. Color and thickness of the bar indicate lateral velocity of a particular segment of the fin. The beat frequency for each fin is the same, 4.9±0.3 Hz. (A) Caudal fin kinematics. Note how the upper and lower lobes bend into the flow at stroke reversal. Inset shows position of the two planes. (B) Dorsal and anal fin kinematics. Note the cupping motion of the outer edges of each fin. Scale bars are the same for A and B.

Streamwise vortex structure

A primary result of this study is the identification of streamwise vortices formed at different points along the fish's body. Vortices shed at eight locations along the fish's body were identified (Fig. 4): the dorsal and ventral tips of the caudal fin, the angled ventral edge of the dorsal lobe of the caudal fin (the upper caudal fin notch), the dorsal edge of the ventral lobe of the caudal fin (the lower caudal fin notch), and the dorsal and ventral edges of both the soft dorsal fin and the anal fin. Additionally, vortices were tentatively identified as being shed off the dorsal and ventral edges of the caudal peduncle, although they were difficult to identify definitively because the caudal fin often blocked the view of the peduncle. Vortices from the pectoral fin were also observed as they convected through the light sheet, but are not included in the present analysis. Outer vortices from the anal and dorsal fin could be identified in posterior planes by their phasing and position. Other vortices, including those from the peduncle and the inner edges of the anterior median fins, could not be identified definitively as they convected toward the caudal fin. Vortices unidentified in posterior planes (such as the unlabeled vortices in Fig. 4A) may thus have been formed by the peduncle or the inner edges of the dorsal and anal fins, or by other sources such as the pectoral and pelvic fins.

The record of these vortex patterns over time could be used to construct an approximation of the 3D streamwise wake structure using the mean flow passing through the transverse planes. From the flow's viewpoint, the light sheet can be imagined as moving forward through still water, following the fish as it swims, and thus sampling a range of positions, rather than a range of times. Fig. 5 shows such an approximation on

the basis of a light sheet at the tip of the caudal fin. Most unidentified vortices were observed near the horizontal midline and, while they typically had lower circulations than identified vortices, together they make up a substantial component of the total circulation. Some asymmetry is also present; for example, only clockwise vortices from the dorsal fin were detected, an asymmetry like that which Standen and Lauder (Standen and Lauder, 2005) also found in dorsal fin kinematics.

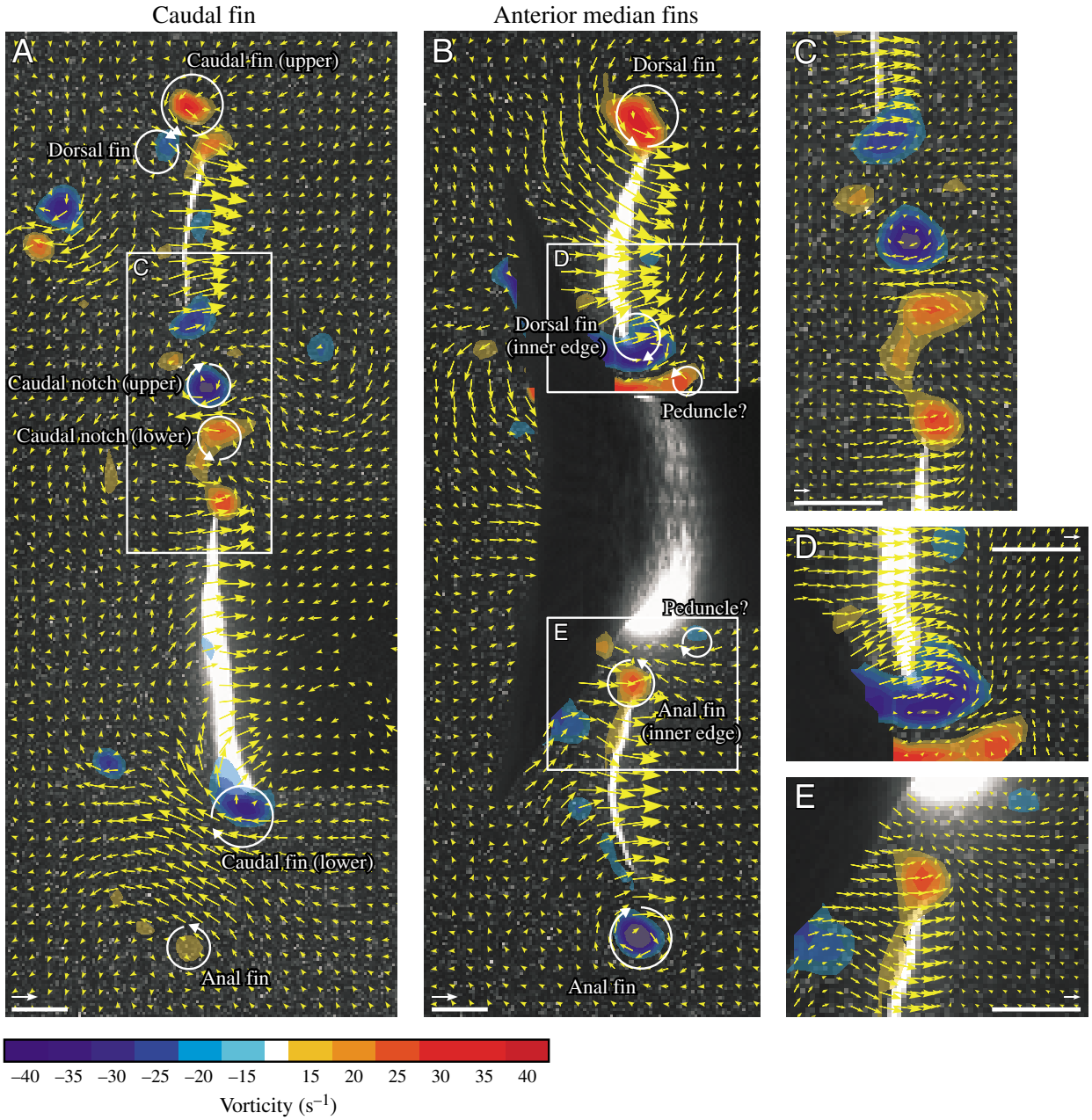

Fig. 4. Examples of each of the ten different vortices identified. All images have the original PIV image in the background, yellow vectors represent the flow field, and vorticity is shown as colored contours. In all panels, scale bars are 5 mm and scale vectors are 5 cm s^{-1}. The heads of vectors shorter than 3 cm s^{-1} are retained to indicate direction. (A) Flow field at the posterior margin of the caudal fin, with the laser illuminating the upper and lower lobes of the fin. The tail is moving from left to right and has just formed the two tip vortices, labeled 'caudal fin (upper)' and 'caudal fin (lower)'. Weak remnants of the outer dorsal and anal fin vortices are still present, labeled 'dorsal fin' and 'anal fin'. The notch between the two lobes of the caudal fin also sheds vortices, labeled 'caudal notch (upper)' and 'caudal notch (lower)'. Every other vector is shown. (B) Flow field at the trailing edge of the dorsal and anal fins, with the laser illuminating the two fins and part of the caudal peduncle. The caudal fin blocks the view of some of the flow field. The fins are finishing motion from left to right, and the peduncle has just begun to move from right to left. Outer vortices from the dorsal and anal fins are fully developed (labeled 'dorsal fin' and 'anal fin'). The fins have also formed vortices on their inner edges, labeled 'dorsal fin (inner edge)' and 'anal fin (inner edge)'. Two vortices may have been shed from the peduncle (both labeled 'peduncle?'), but it is difficult to be certain because of the shadow cast by the peduncle. (C–E) Insets showing details of the vector fields boxed in A and B. All vectors are shown in these panels.

This view differs from a true 3D flow field in two primary ways. First, it includes only streamwise vortices, which is not possible in a real fluid. By the Helmholtz vortex theorem, these vortices must be connected in some way to form complete loops (Faber, 1995). Second, it assumes that vortices do not interact with one another and do not evolve over time. Although such evolution and interaction is known to occur (e.g. Tytell, 2004), the view presented in Fig. 5 is still useful for understanding the 3D positions of streamwise vortices.

To verify that vortices identified in posterior planes as dorsal or anal fin vortices were genuinely formed by the dorsal or anal fins, the timing of peak circulation was investigated (Fig. 6). Position alone was not enough to identify the dorsal fin vortex unambiguously. Fish often swam with their dorsal fins slightly lowered and with their heads pitched somewhat downwards; as a result, outer dorsal fin vortices often appeared on the same dorso-ventral level as the caudal fin tip vortex, or sometimes even lower (Fig. 6A). For the same reason, the outer anal fin vortex was typically much lower than the corresponding caudal fin vortex and could be identified unambiguously by its position (Fig. 4A). For verification of the dorsal fin vortex, note that fluid should flow from the trailing edge of the dorsal fin at approximately 70% of body length to the tip of the caudal fin over a time (0.3*L*)/*U*. Flow acceleration in this region of the body is probably negligible and will never be larger than the 20% of *U* observed in the wake by Drucker and Lauder (Drucker and Lauder, 2001). Fig. 6B shows the timing of the dorsal fin vortex circulation as measured at 0.7*L* and at 1.0*L*, showing that they are separated by the correct amount of time.

Spatial changes in circulation

A goal of this study was to examine how overall circulation changes along the body, because circulation is approximately proportional to force. To determine how much circulation changes in a given plane, though, the circulation that convects in from planes further upstream must be removed. This requires taking the derivative with respect to body position. However, the raw data were too noisy to differentiate directly; therefore, a smooth regression model of the vortex circulation was developed.

Separate regressions were performed on circulation from each the vortices, including evolution over time as well as space. This regression indicated that some circulation may indeed decrease at the base of the caudal fin. A coordinate system that follows the mean flow was chosen. The assumption that vortices progress down the body at mean flow speed was tested in two ways. First, the position and time of peak vorticity of each vortex was plotted and compared visually to the flow speed and body wave speed. Vortex speed was much closer to flow speed than body wave speed (for an example, see Fig. 7A). Second, the regression models used (Eqn 4 and 5) allow some variation in vortex speed around the flow speed (i.e. phase can change nonlinearly along the body; see Materials and methods for an explanation).

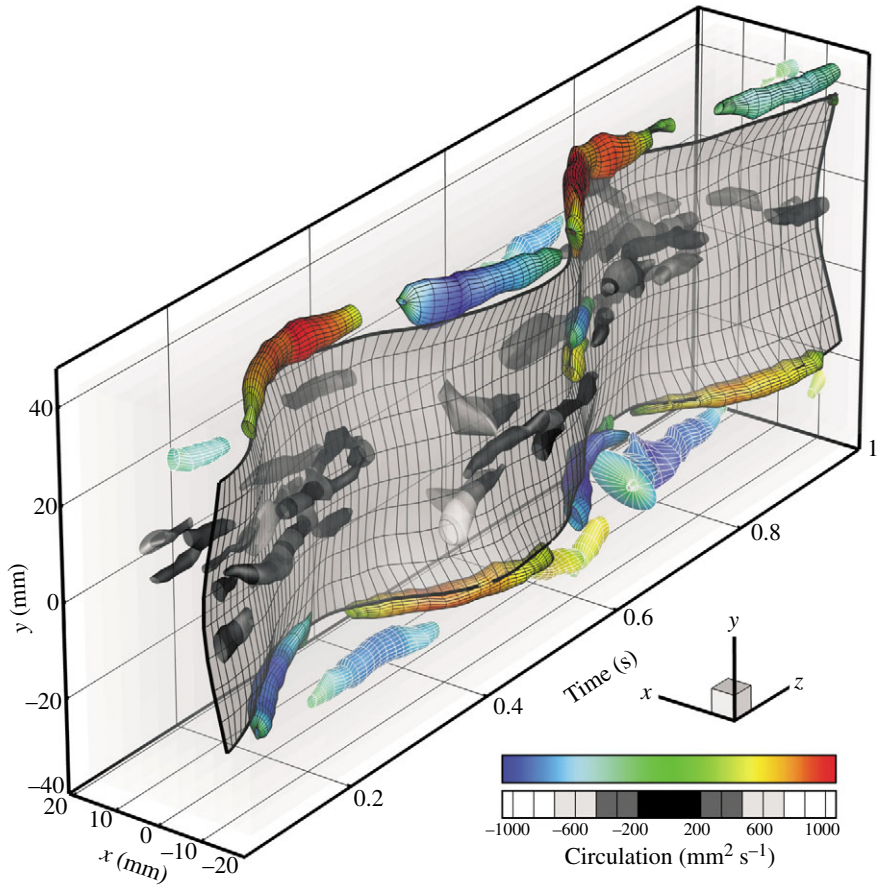

Fig. 5. Pseudo-three-dimensional view of the wake, showing the *x* and *y* positions of vortices detected at the tip of the caudal fin, with time as the third axis. This view is representative of the streamwise vortices in the wake if the vortices did not evolve over time or interact with each other. The sheet swept out by the caudal fin is shown in gray. Identified vortices are colored by circulation, while vortices that were detected but whose source could not be determined are shown with shades of gray representing circulation. Vortices shed by the caudal fin, including the two tip vortices and the caudal notch vortices, have a black mesh, while the outer dorsal and anal fin vortices have a white mesh.

In the regressions, vortex circulation was polynomial over position and periodic over time. With linear changes in amplitude and one Fourier mode (Eqn 4), the mean r^2 value was 0.61 (range 0.4–0.72). Quadratic amplitude terms (Eqn 5 with n=2 and m=1) were mostly significant, but only increased mean r^2 to 0.64 and began to introduce undesirable effects at the ends of the ranges as the quadratic terms increased rapidly. Additionally, the second order Fourier modes (Eqn 5 with n=1 and m=2) were mostly not significant (22 out of 32 terms were significant), small in amplitude (below 400 mm^2 s^{-1}), and increased the mean r^2 only slightly (to 0.63). Higher order oscillations may be present in reality, but could not be detected through the noise. Thus, a linear amplitude change with a single Fourier mode (Eqn 4) was deemed sufficient.

Interaction with the body appears to change the observed circulation of individual vortices as they move with the flow (Fig. 7B). The measurements in this study cannot distinguish

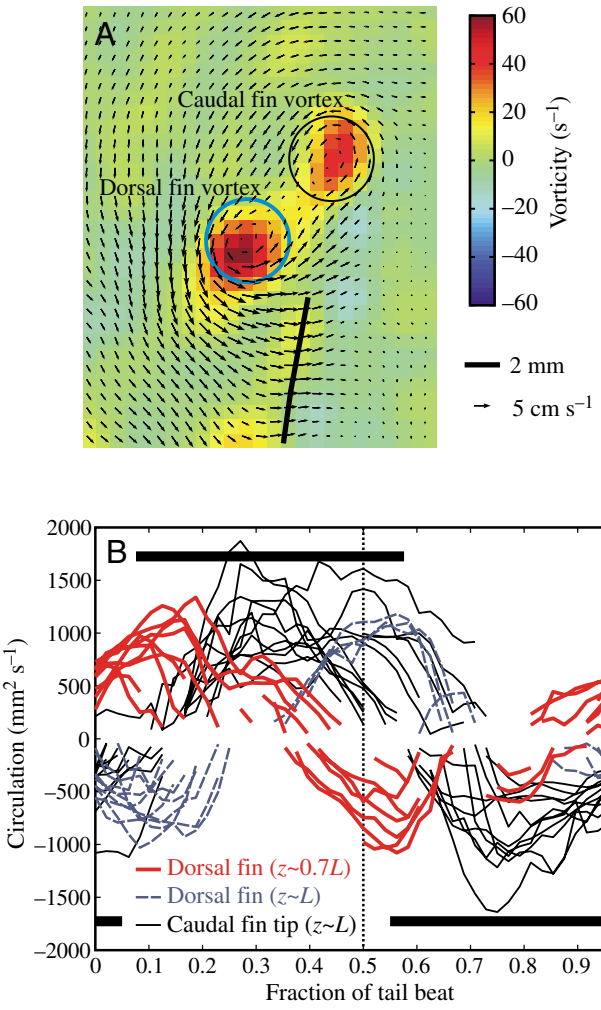

Fig. 6. Identification of outer dorsal fin vortex in the wake. (A) Two vortices above the upper margin of the caudal fin in a plane approximately 5 mm downstream of the tail, shown by a thick black line. The caudal fin vortex appeared first and is clearly a tip vortex from the caudal fin. The lower vortex, labeled 'dorsal fin vortex', appears later. (B) Plot of the circulations of three vortices against tail beat phase. Red line, outer dorsal fin vortex as it is formed on the dorsal fin at z≈0.7L; broken blue line, lower vortex in (A) at z≈L; thin black line, caudal fin tip vortex (upper vortex in A), at z≈L. Black bars indicate the length of time it would take flow to pass from the posterior margin of the dorsal fin to the tip of the tail, positively identifying the blue trace as the outer dorsal fin vortex. Dotted vertical line indicates the time of A.

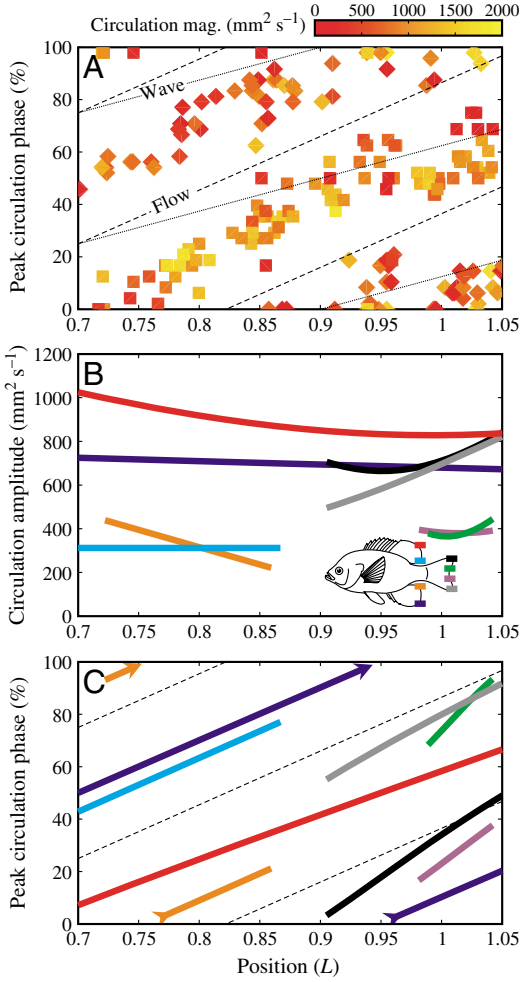

Fig. 7. Mean vortex circulation changes along the body. All plots have the same x axis: body position in L. (A) Example of raw data used for the vortex circulation. Peak positive and negative circulation for the dorsal fin vortex are shown. Color indicates circulation magnitude (mag.); squares and diamonds are from positive and negative circulation vortices, respectively. Broken and dotted lines indicate flow speed and wave speed, respectively, and are spaced 50% of the tail beat cycle apart. (B,C) Results of the regression of circulation on phase and body position, detailed in Eqn 4, showing the amplitude of the oscillation in circulation (B) and the phase of the positive circulation peak (C). Line color indicates specific vortices, shown schematically at the bottom of B. Phase trajectories in C that wrap around from 100% back to 0% are indicated with arrowheads and -tails. Although the regression from Eqn 4 is linear in the amplitude of the sine and cosine terms separately, the joint amplitudes and phases can have nonlinearities due to the differing weights of the coefficients. See text for more details.

vortex reorientation (i.e. streamwise vortices becoming more vertical, or *vice versa*) from true changes in circulation, but both effects may be results from interactions with the body. All vortices except for the inner dorsal fin vortex had significant changes in circulation along the body (P<0.05 in all cases; Fig. 7B). The circulation oscillations were slightly asymmetric for all the major vortices (outer dorsal and anal fin vortices and both caudal fin tip vortices), meaning that the C parameters (intercepts) from Eqn 4 were significant. The intercepts were less than 12% of mean amplitude in all cases, but did show a bias towards stronger vortices on the fish's left, probably reflecting the fish's desire to escape the experimenter or the bright laser light, which were both on its left.

Fig. 7C shows the phase of the peak positive circulation as each vortex moves down the body. Most vortices track with the mean flow speed (shown with broken lines), although the caudal fin vortices have a velocity slightly (but significantly; P<0.05 in all cases) above mean flow, probably reflecting the acceleration of flow near the caudal fin.

The magnitude of circulation from each vortex, estimated through these regressions, was summed and differentiated along the body position. This allowed an estimate of the streamwise circulation added by each point along the body. Fig. 8 shows the estimated total circulation and its derivative. Note that circulation decreases near the caudal peduncle and occasionally along the caudal fin itself (blue regions in Fig. 8B). The mean circulation added over the whole tail beat period was estimated for 12 segments from 0.7 to 1.0L, each with length 0.025L (Fig. 9).

Fig. 9 indicates that circulation is added primarily at three points: at the trailing edges of the dorsal and anal fins, about halfway down the caudal fin, and at the very tip of the caudal fin. These correspond to the dorsal and anal fin vortices, the creation of the caudal fin tip vortices, and the vortex shedding from the notch in the caudal fin. In contrast, the caudal peduncle and the base of the caudal fin appear to remove circulation, possibly indicating some vortex interaction between the caudal fin and the dorsal and anal fin vortices. Note that Fig. 8B shows a small region of circulation loss at near 0.95L; however, averaged over a full tail beat, this region of the body does add net circulation, as Fig. 9 shows. The pattern and approximate magnitudes shown in Fig. 9 were robust to all changes of polynomial and Fourier order in the regression model described above.

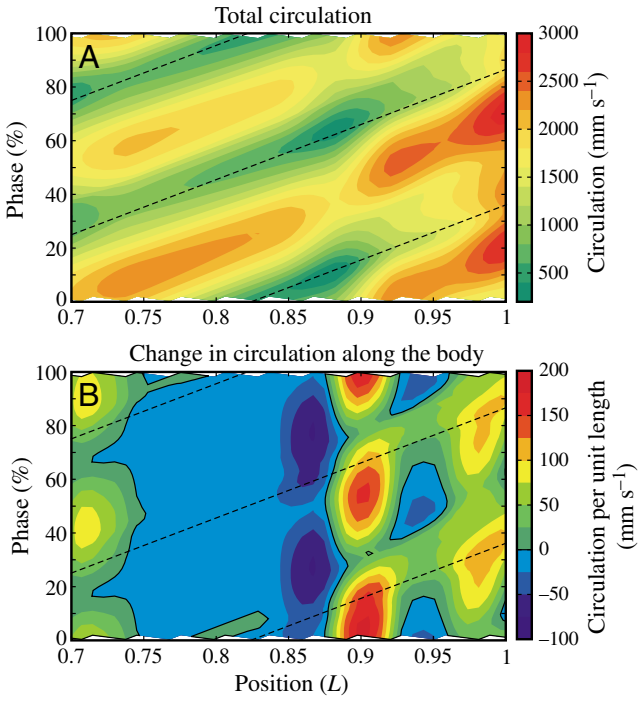

Fig. 8. Sum of the regressions for each individual vortex's circulation to determine how total circulation changes as flow moves down the body. Broken lines on each plot indicate the slope of the flow speed; they are only visual guides and are not fit to the data. (A) Total circulation magnitude along the body over the tail beat cycle, composed of the smoothed sum of the fitted circulations for each identified vortex. (B) Magnitude of circulation added per unit length by each position on the body over half of a tail beat cycle, estimated by taking the derivative of A with respect to position along the broken lines of flow speed. The zero contour is outlined in a thin solid black line, indicating that circulation is removed at certain times and places.

Comparison of circulation among vortices

Finally, the peak circulations of vortices from each fin were compared using a two-way, mixed-model ANOVA with

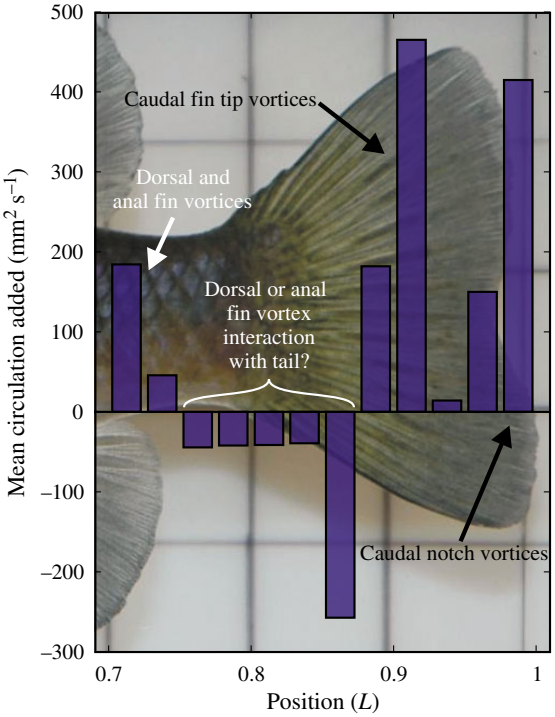

Fig. 9. Averaged over a tail beat, circulation increases at the dorsal and anal fins and at the trailing edge of the caudal fin, but decreases at the caudal peduncle and base of the caudal fin. Bars show mean circulation added over a tail beat at 12 points along the body, each 0.025L wide.

effects from vortex type (fixed effect) and individual (random effect). Table 1 summarizes the results, and the least-squares means of the peak circulation of each vortex are given in Fig. 10. Multiple comparisons of the vortex strengths (using Tukey's honestly significant difference) show that, with 95% confidence, the two caudal fin tip vortices are not significantly different from one another or the outer dorsal fin vortex, while the outer anal fin vortex is not significantly different from the lower caudal fin tip vortex. The two vortices from the caudal fin notch are not significantly different, either, but the outer dorsal fin vortex is significantly stronger than the outer anal fin vortex.

Comparison to 2D ideal flow

Fig. 11 shows an example of the effectiveness E of the tail in accelerating flow in a single direction, based on Eqn 8. Fig. 11A,B show examples of the flow accelerated up and down as the tail moves from left to right and from right to left, respectively. Because of the shadow cast in the laser light sheet, E could only be estimated on one side of the tail at a time (termed 'single-side effectiveness'). By using the flow estimates from sequential half tail beats, a total effectiveness was estimated. Fig. 11C shows both the single-side effectiveness and the estimated total effectiveness for four example tail beats. The mean peak value of E for the 32 half tail beats near the tail tip ($0.975L \leqslant s \leqslant 1.025L$) was 0.75±0.02.

Discussion

In this study, I describe the streamwise vortex structure around the posterior body of a swimming bluegill sunfish *Lepomis macrochirus*. To my knowledge, these are the first observations of streamwise vorticity near the tail of any swimming fish, and only the second time flow in the transverse plane has been observed in a biological fluid dynamic study (the first was Drucker and Lauder, 1999). Additionally, because flow in this plane was sampled at multiple points along the body, this study provides the most complete experimental description to date of three-dimensional flow around a swimming fish.

Table 1. *ANOVA on maximum vortex circulation*

Source	MS	d.f.	F	P
Vortex	**2 524 531**	**7**	**11.48**	**<0.0001**
Denom: $0.97Fs\times Vx+0.03\epsilon$	219 869	21.5		
Fish (random)	83 646	3	0.5	0.684
Denom: $0.57Fs\times Vx+0.43\epsilon$	167 133	35.39		
Fish×Vortex (random)	**223 540**	**21**	**2.43**	**0.0004**
Error	92 038	668		

N=700. Bold indicates a significant effect.

MS, mean square; d.f., degrees of freedom.

Denominators (Denom.) used for F tests shown below relevant effects, where $Fs\times Vx$ is the Fish×Vortex MS error and ϵ is the residual error; when not listed, the error MS was used.

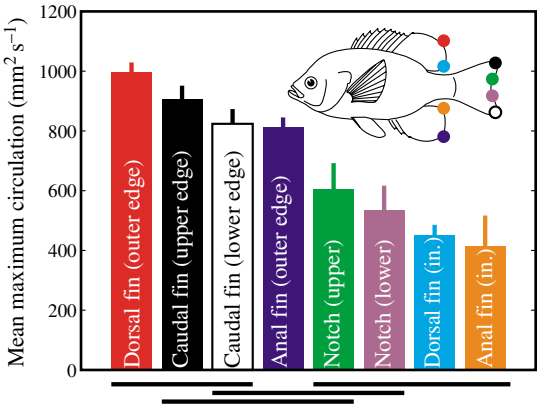

Fig. 10. The dorsal and anal fins produce vortices with streamwise circulation statistically indistinguishable from those produced by the caudal fin. Bars show the mean + s.e. of the peak circulation over the entire body, based on the ANOVA described in the text. Vortices with circulations that do not differ significantly (P<0.05) are connected by bars below the plot. Inset shows the position on the body where each vortex was generated.

Three-dimensional vortex structure

Transverse flow patterns are quite complex. Streamwise vortices are shed off the caudal fin, at the dorsal and ventral margins as well as at the central notched region, and off the dorsal and anal fins, at both the dorsal and ventral margins of each. By the Helmholtz vortex theorem (Faber, 1995), all of these vortices must connect in some way to form loops. In Fig. 12A,B, I propose a 3D wake structure that incorporates the present measurements. Although the pattern is complex, low-aspect ratio flapping foils also show similarly intricate structures (Buchholz and Smits, 2006; Dong et al., 2005; von Ellenrieder et al., 2003). The caudal notch vortices connect to form something like a hairpin vortex within the overall vortex ring. The tail's cupping motion elongates them more than might be expected from the shape of its trailing edge, but they do not appear to connect to form a full 'ring-within-a-ring' structure, observed by Wilga and Lauder from shark tails (Wilga and Lauder, 2004).

In retrospect, the size and shape of these hairpin notch vortices could have been predicted from kinematics alone, going back to Bainbridge's measurements from dace *Leuciscus leuciscus* (Bainbridge, 1963), and Lauder's observations from sunfish (Lauder, 2000). Both observed approximately the same tail motion seen in this study: a distinct cupping motion, in which the center of the fin moves only about 60% as far as the tips and lags behind the tips by about 9% of the tail beat cycle (Fig. 3). Because of these amplitude and timing differences, the vertical vortices from the center of the fin must be in different places than those from the upper and lower edges (as shown in the horizontal projection of Fig. 12).

Although the vortex structure proposed appears much more complex than previous portrayals (e.g. Lauder, 2000), it is consistent with them. Any horizontal section would find two

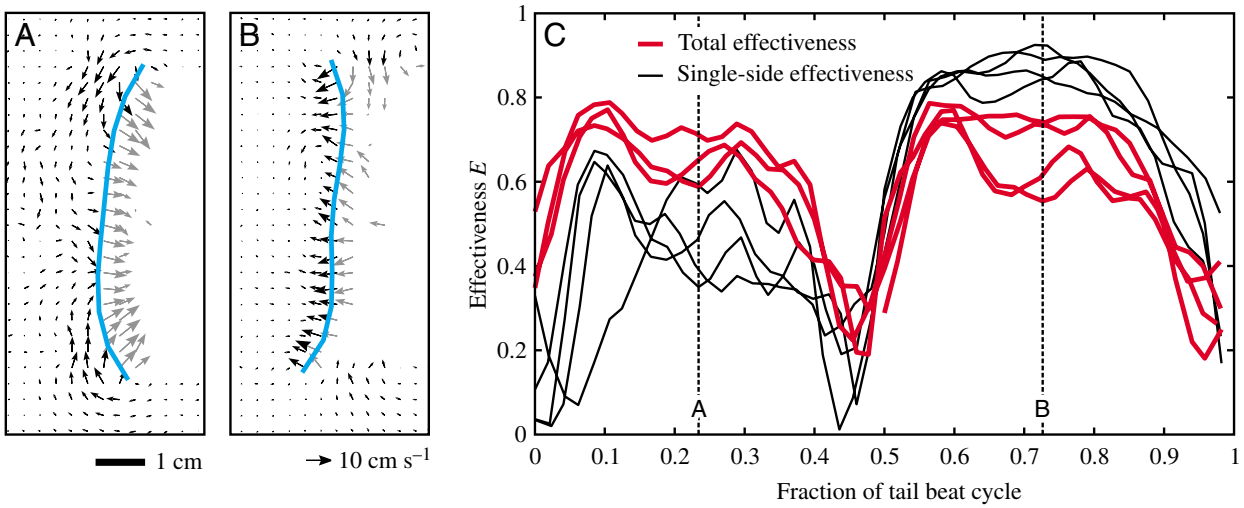

Fig. 11. Representative plot of the geometric effectiveness E measured at 0.95L, with example flow fields at approximately 25% and 75% through the tail beat cycle. (A,B). Example flow fields showing the main flow patterns as the tail moves from left to right (A) and from right to left (B). The tail is shown in blue. Scale bars and scale vectors shown below the panels are valid for both. Light passes through the tail to a small extent, allowing the estimation of some vectors in the shadowed (right) side, but these vectors, shown in gray, were not used in the effectiveness calculations. (C) Effectiveness estimated assuming tail beats are symmetrical (red line) by using the previous half tail beat to reconstruct flow in the shadowed side of the tail. The black line shows the single-side effectiveness, using only the flow on the illuminated side of the tail. Single-side effectiveness is higher in the first half of the tail beat, showing that the tail is less effective at sucking fluid laterally than it is at pushing it, probably due to its cupped shape. The dotted lines show the times at which A and B were measured.

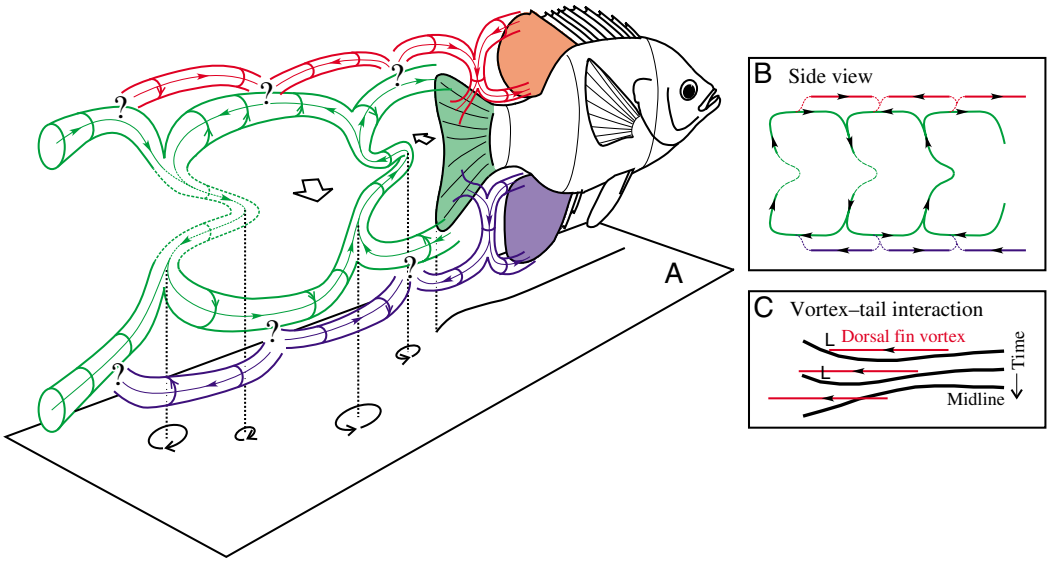

Fig. 12. Proposed 3D vortex structure around a swimming bluegill sunfish. Vortex loops are shed off the caudal, dorsal and anal fins, shown in green, red and blue, respectively. Vortex filaments and their directions are shown by solid arrowheads. The direction of vortex rotation, derived by the right hand rule from the filament direction, is shown with open arrowheads where there is space. (A) 3D view, showing the proposed linkages between caudal fin tip vortices and dorsal and anal fin vortices. Question marks are shown where the connection between dorsal or anal fin vortices and the caudal fin wake is unclear. The notch vortices in the far wake are shown by dotted lines, indicating that the structure is hydrodynamically unstable and may not persist in the form shown. A projection of the vortex structure in the horizontal plane is shown below, with dotted lines indicating the correspondence between the projection and four centers of rotation. Note that the projection is taken from multiple horizontal planes. A midline tracing, in the correct phase, is shown below the fish. (B) Side views of the vortex filaments shown in A as the fish swims from left to right, showing how the dorsal and anal fin vortex filaments could potentially join up to the caudal fin vortices. Notch vortices in the far wake are again shown dotted to indicate their instability. (C) Schematic of the progression of the outer dorsal fin vortex and its interaction with the caudal fin, shown at three points in time from top to bottom. The fish is holding station in flow moving from right to left. L, low pressure zones that would be formed along the tail due to the proximity of the outer dorsal fin vortex.

strong centers of vorticity arrayed in a reverse von Kármán street, as observed for carangiform swimmers (Drucker and Lauder, 2001; Müller et al., 1997; Nauen and Lauder, 2002a), and vertical sections would find two tip vortices for most of the cycle (Nauen and Lauder, 2002a; Nauen and Lauder, 2002b). It is also numerically consistent with Drucker and Lauder's results from similar-sized sunfish swimming at about the same speed (Drucker and Lauder, 2001). Estimated from their published figures, sunfish swimming at 1.1 L s^{-1} produce vertical vortices from the caudal fin with circulations near 1000 mm^2 s^{-1}, comparable to the measured streamwise vortex circulations.

However, Fig. 12 makes several easily tested predictions of effects that have not previously been observed. In particular, there should be a shift in the timing and spacing of vertical vortices among horizontal planes at the midline *versus* upper or lower planes, as indicated by the horizontal projection in Fig. 12A. Additionally, observations of flow in a vertical plane should identify the caudal notch vortices.

Do these notch vortices have a functional significance? Wilga and Lauder proposed that the ring-within-a-ring structure from a shark's tail might enhance maneuverability, by allowing sharks to tune the force production precisely (Wilga and Lauder, 2004). The caudal notch vortices may be the evidence of similar abilities in the sunfish; namely, each lobe of the caudal fin is independently controlled and can produce different forces. In steady swimming, the caudal notch vortices are equal in strength (Fig. 10), but they need not be. An imbalance in the two vortices would allow fine tuning of pitching and rolling moments produced by the tail during steady swimming. Larger imbalances might be used during maneuvers.

The notch vortices also have a disadvantage: they cause the tail to transmit force less efficiently. A circular vortex ring would be more efficient at producing thrust than the loop shown in Fig. 12 (Lighthill, 1970). Thus, the vortices may be evidence of a trade-off between maneuvering capabilities and swimming efficiency.

The mechanical properties of the tail and its kinematics may determine whether caudal notch vortices are produced. Nauen and Lauder, using PIV in a vertical plane, did not observe these vortices from mackerel (Nauen and Lauder, 2002a), despite the deep fork in their tails. One explanation is that their measurements may have lacked the resolution necessary to detect these vortices (they estimated approximately 20 vectors over the tail height, while about 90 vectors were estimated in this study). More interestingly, though, if mackerel genuinely do not produce caudal notch vortices, it may indicate the different specializations of mackerel and bluegill sunfish. Mackerels' stiffer tails and lack of the cupping motion (Gibb et al., 1999) may allow them to produce a more efficient, more circular vortex ring wake, better suited to steady long distance swimming. Additionally, the higher aspect ratio of their tail fin may mitigate some of the 3D losses, estimated with E. Sunfish, in contrast, may sacrifice some propulsive efficiency for a less-rigid tail that enables them to maneuver more precisely.

It should also be noted that the notch vortices, while convincingly shown in the near wake (Fig. 4A,C), are not hydrodynamically stable. The notched vortex loop depicted in Fig. 12 assumes little interaction between them over time, which is probably not a valid assumption. Thus, in the far wake, the 3D structure is less clear (indicated by broken lines in Fig. 12). However, the functional consequences of the wake depend primarily on the near wake; the temporal evolution of the wake has a relatively small effect on the fish's swimming.

Fig. 12 also incorporates a more speculative idea of the 3D structure of the dorsal and anal fin vortices, shown in red and blue, respectively. The results of this study (Fig. 5), combined with Drucker and Lauder's horizontal measurements near the dorsal fin (Drucker and Lauder, 2001) clearly indicate that these vortices first form as part of small linked vortex rings from each fin. However, the inner portion of the ring is probably destroyed by interactions with the caudal fin (as Fig. 9 suggests). To maintain a hydrodynamically consistent vortex filament structure, the outer portions must link up with the caudal fin vortices in some way. It is difficult to find a consistent structure with links between these and the caudal fin vortices (indicated by question marks in Fig. 12A), but Fig. 12B shows one hypothesis.

A different explanation for the difficulty in constructing a vortex filament model is that the model itself may not be consistent with such complex flows. The interaction of flow from the anterior median fins as it passes over the caudal fin may not be reducible to a simple small-core vortex model. The fins actually shed distributed sheets of vorticity, which may be approximated in some cases as simple filaments, but the interaction between the streamwise vortices shed off the tip of the caudal fin and the outer edges of the dorsal and anal fins may be too complex for such a representation. Further measurements near the caudal peduncle and in the wake will clarify the structure.

Vortex interactions

Many previous studies have proposed that vortices produced on the anterior body might interact with flow around the caudal fin, potentially boosting the fin's thrust or efficiency (Ahlborn et al., 1991; Gopalkrishnan et al., 1994; Wolfgang et al., 1999; Zhu et al., 2002). Drucker and Lauder found the first empirical evidence of such interactions (Drucker and Lauder, 2001; Lauder and Drucker, 2004), and Akhtar and Mittal used a computational simulation to demonstrate that the interaction doubled the caudal fin's thrust and increased efficiency by 50% (Akhtar and Mittal, 2005).

This study provides evidence for vortex interactions in the streamwise direction, a previously unrecognized source of vortical flow that might be exploited by the caudal fin. Figs 8B and 9 indicate that the observed streamwise circulation decreases as flow moves from the anterior median fins over the peduncle to the caudal fin. The vortices from the inner margins of the dorsal and anal fins almost certainly interact with the tail in this region (indicated schematically in Fig. 12), and, if the two fins are depressed slightly more than Fig. 12 depicts (as is

common at higher speeds; Drucker and Lauder, 2001), the fins' outer vortices may also intersect the tail. The estimated decrease may be due to four different effects: (1) difficulty in observing vortices near the peduncle; (2) viscous or turbulent dissipation of vorticity; (3) reorientation of streamwise vortices to a more vertical or lateral orientation; (4) true reduction in circulation of the vortices.

First, the region where circulation seems to be removed (from 0.75 to 0.875L in Fig. 9) was also the most difficult region to resolve vortices, because the caudal fin often blocked much of the view. Some of the decrease, then, may be attributable to methodological difficulties in observing flow near the peduncle.

Second, this decrease could also be due to viscous or turbulent dissipation of vorticity (Tytell and Ellington, 2003), but the diameter of the vortex cores did not change substantially, as would be expected with viscous diffusion of vorticity, nor did the vortices appear to be breaking up turbulently. The length scale for viscous diffusion, $\sqrt{\nu T}$, where ν is the kinematic viscosity and T is the tail beat period, is about 0.6 mm, which is sufficiently smaller than the average vortex core radius (around 2.5 mm for the major vortices) for viscous diffusion of vorticity to be a minor effect (Saffman, 1992).

Thus, it seems likely that the decrease in circulation is not due to evolution of the flow itself, but rather to the third or fourth effect, reorientation or true decreases in circulation. Both of these are the results of interactions with the body. These interactions may simply reduce the amount of circulation measured, without changing the true total circulation, or may genuinely reduce overall circulation. First, the body may cause streamwise vortices to become more vertical, reducing the circulation measured in the transverse plane. Also, the body may destroy a vortex as a coherent structure, without actually changing the total vorticity in the flow, by causing the vortex to break down turbulently. Small regions of vorticity would not be detected by the vortex identification algorithm, or might drop below the error threshold in PIV. Vortex flow may also be incorporated into the boundary layer vorticity, removing the vortex as a separate flow structure, but maintaining overall circulation. Alternatively, however, the high pressure region on the anterior surface of the fin may raise the low pressure region in the center of the vortex, spreading out the vortex core and truly reducing its strength.

The final effect implies that the fish may be able to exploit the above interactions for its own benefit. Based on the body and vortex kinematics, I hypothesize that fish may be able to increase the thrust of the caudal fin by reducing the pressure on the anteriorly inclined surface. Pressure in the center of a vortex is low (Faber, 1995). As streamwise vortices from the dorsal and anal fins pass near the caudal fin, they will reduce the pressure on the side that is angled forward, while the pressure in the center of the vortex becomes closer to ambient, reducing the vortex circulation. The kinematics are consistent with this proposal (shown schematically in Fig. 12C), but more study, particularly computational simulations (like those of Akhtar and Mittal, 2005), will be necessary to determine whether any thrust augmentation is present and how important an effect it is.

Even if the effect is present, the fish does not receive something for nothing. The dorsal and anal fin vortices may increase the caudal fin's thrust, but the efficiency of the entire fish will still be much lower than one. In fact, a more efficient arrangement would have been not to create the dorsal and anal fin vortices in the first place, because the energy used to create them will never be completely recaptured by the caudal fin. However, because the anterior median fins are clearly useful for other purposes, such as maneuvering and roll stability (Drucker and Lauder, 2001; Standen and Lauder, 2005), recapturing some of their vortex energy at the caudal fin could improve steady swimming, despite competing functional demands.

Importance of the dorsal and anal fins

Not only do the soft dorsal and anal fin possibly increase the efficiency of the caudal fin, but they produce considerable forces themselves. In fact, the vortex data in this study suggest that they produce a combined force that is comparable to that of the caudal fin. In steady vortical flow, like a vortex ring, the force that produced the flow is proportional to the vortex's circulation and the area of its loop (Batchelor, 1973). While this assumption does not necessarily hold in complex unsteady flows like fish swimming (Dabiri, 2005), estimations of thrust and lift forces, for example, on the basis of this method have at least been consistent with measured drag and weight forces (Drucker and Lauder, 1999). Additionally, studies of birds using a steady vortex analysis (Spedding et al., 2003; Warrick et al., 2005) found good agreement between the circulation required to support a flying bird and the circulation they measured in the wake.

Therefore, the relative magnitude of forces produced by the median fins can be compared by examining the relative circulations of the vortices they produce, as well as the areas of the vortex loops. Fig. 10 shows that the streamwise circulation produced by each of the three median fins is not significantly different. Their circulations in the vertical direction are probably also comparable, at least at the moment it is shed, because a vortex filament must form a continuous loop connecting the opposite sense streamwise vortices (Faber, 1995). Therefore, the loops probably have roughly the same circulation in all planes. The horizontal plane flow fields presented by Drucker and Lauder (Drucker and Lauder, 2001) are also consistent with this observation. Additionally, the areas of the fins' respective vortex loops are also comparable. Loop area, in turn, is approximately equal to the product of the streamwise diameter and the dorso-ventral height. Loops from the dorsal fin, anal fin and caudal fin have approximately the same streamwise diameter (Fig. 5), because the beat frequency is the same. With reference to the picture in Fig. 9, the combined trailing edges of the erected soft dorsal and anal fins are quite comparable to that of the caudal fin. Thus, the combined areas are also similar, and the vortices' contribution

to total force should also be comparable to that of the tail. Probably the forces are within a factor of two of each other, and are almost certainly the same order of magnitude. As propulsors, the dorsal and anal fins together are approximately equal to a second tail.

Drucker and Lauder's results from the horizontal plane (Drucker and Lauder, 2001) support this argument. They found that the soft dorsal fin produced a substantial amount of thrust: about 40% of that produced by the caudal fin. They did not have measurements from the anal fin, but on the basis of the fact that the kinematics are similar (Standen and Lauder, 2005), one would expect that horizontal measurements from the anal fin would show similar amounts of thrust. Together, force from the two fins would thus be nearly equal to that from the tail.

The above arguments highlight the importance of the dorsal and anal fin relative to the caudal fin. They should not be construed as a statement that the anterior median fins produce forces that exactly equal those of the caudal fin. First, as discussed above, they neglect unsteady effects. Secondly, the argument hinges on a rough evaluation of the length of the trailing edges of the fins. Fish can control these lengths actively by erecting or depressing the fins (Helfman et al., 1997). Particularly at high speeds, the dorsal and anal fins will not be fully erected and therefore will produce lower forces. Finally, the argument does not relate to the direction of the forces. The caudal fin may well produce substantially more thrust than the dorsal and anal fins (Drucker and Lauder, 2005), even if the total force magnitudes are comparable. Nonetheless, the observations in this study indicate that the combined dorsal and anal fin force is comparable to that of the caudal fin, within an order of magnitude, and possibly much closer for bluegill sunfish swimming at low speeds.

Additionally, the division of forces between the dorsal, anal and caudal fin in other fish taxa may not be as symmetrical as observed in bluegill sunfish, a percomorph fish. For example, the dorsal fin in trout, a basal euteleost, is placed much more anteriorly than their anal fins (Helfman et al., 1997) and seems to produce primarily lateral forces (Drucker and Lauder, 2005). The anal fin, which is comparable to the dorsal fin in size, probably also produces large forces, but the relative magnitude and timing (important for balancing roll moments; Standen and Lauder, 2005) has not been described. In contrast, eels, basal teleosts, have dorsal and anal fins that merge into the caudal fin (Helfman et al., 1997; Lauder and Tytell, 2006), and thus do not have a separate vertical trailing edge. They will still shed streamwise vortices, but the structure of these vortices is currently unknown. Comparative studies are necessary to determine the hydrodynamic effect of these different fin placements.

Nonetheless, in many fish taxa, it is likely that the dorsal and anal fins play an active and substantial role in steady 'body and caudal fin' swimming, which is usually separated from 'median and paired fin' swimming (Helfman et al., 1997). The current observations and those of Drucker and Lauder (Drucker and Lauder, 2001; Drucker and Lauder, 2005) and Standen and Lauder (Standen and Lauder, 2005), indicate that this division is not so clear, and should perhaps be revised.

Three-dimensional fish, two-dimensional theories

A clear conclusion from this study is that the two-dimensional view of fish swimming misses several important effects, most notably the contributions of the dorsal and anal fin. Most 2D theories (except for, for example, that of Weihs, 1972) neglect these two fins entirely, passing over a sizeable fraction of the total force and a potential method to enhance thrust from the caudal fin. Additionally, the 3D motion of the caudal fin may have important functional consequences for maneuverability.

Numerically, Fig. 11 indicates that the caudal fin is only about three-quarters as good at accelerating flow in a coherent direction as a 2D plate. At best, about 25% of the flow near the tail tip is present as up and down momentum that cancels out, resulting in zero net force. In fact, the cupping motion of the tail may be an attempt to reduce this effect; on the cupped side, E is increased to approximately 90%. More anterior regions of the body, which are more rounded and cannot cup into the flow, probably have even lower E values.

One should be cautious in relating the effectiveness E to Froude propulsive efficiency. While the losses due to opposing momentum will lower the propulsive efficiency, E cannot be used as a numerical estimate of Froude efficiency. Instead, it is intended to assess the 'two-dimensionality' of a 3D shape and flow pattern, to be used as a guide for the application of 2D theoretical models.

These models will have two opposite types of errors due to effects observed in this study: neglecting the dorsal and anal fins will tend to produce underestimates of 3D forces, while the losses due to cancellation of vertical momentum will result in overestimates. Tytell observed that elongated body theory (Lighthill, 1971) and 2D resistive models (Taylor, 1952) both underestimate lateral forces for eels, possibly indicating that the first effect may be more important than the second (Tytell, 2004). Correcting for this underestimate is not difficult for fishes like sunfish with separate median fins; Weihs provided a method for adding in the contributions from fins other than the caudal fin (Weihs, 1972). For eels, in which the dorsal and anal fin merge into the caudal fin, such a correction is more difficult, because the dorsal and anal fins will produce streamwise vortices but have no vertical trailing edges. Additionally, correcting for the overestimate due to losses from cancellation of vertical momentum is not straightforward. Given these caveats, Weihs's extension to elongated body theory (Weihs, 1972) may still produce useful comparisons of swimming modes and fin sizes and placements, but the numerical force and power estimates should be evaluated cautiously. In particular, Schultz and Webb argue for the use of 2D theoretical models to examine the power requirements of steady swimming (Schultz and Webb, 2002). The current results, in contrast, indicate that 3D computational models (e.g. Dong et al., 2005; Zhu et al., 2002) may be important to produce accurate estimates and that more experimental measurements of 3D flows will be necessary to avoid overlooking important effects, such as the contributions of the dorsal and anal fins.

List of symbols

a_{ij}, b_{ij}	coefficients used to fit circulation in Eqn 4 and 5
C	intercept in the model in Eqn 4 and 5
E	geometric effectiveness, defined in Eqn 8
L	fish length
m	number of Fourier modes in the regression model (Eqn 5)
n	number of polynomial terms in the regression model (Eqn 5)
P	statistical probability
s	arc length along the body midline, starting at the head
$\mathbf{t}$	unit vector tangent to contour
t	time
T	tail beat period
$\mathbf{u}$	flow velocity vector
u	horizontal flow velocity component
U	mean flow (swimming) speed
v	vertical flow velocity component
w	downstream flow velocity component
x	horizontal position
y	vertical position
z	axial (streamwise) position
α	phase of the body's motion, adjusted for the flow speed
Γ	vortex circulation
Γ_{min}	minimum circulation of an automatically identified vortex
λ	threshold swirling strength for vortex identification
θ	angle between the two cameras
ν	kinematic viscosity of water
τ	minimum duration of an automatically identified vortex
ϕ	phase value for the tail tip motion

I am grateful to all members of the Lauder laboratory for helpful discussions of this project, including Peter Madden, who helped with camera configuration and data analysis, and particularly George Lauder. Thanks to Emily Standen, Peter Madden and George Lauder for thoughtful comments on the manuscript. Thanks also to Rajat Mittal for discussions of fluid dynamics. Two anonymous reviewers helped to improve the manuscript substantially. The fish were maintained by Jeremiah Alexander. Funding was provided by NSF IBN0316675 to George Lauder.

References

Adrian, R. J., Christensen, K. T. and Liu, Z.-C. (2000). Analysis and interpretation of instantaneous turbulent velocity fields. *Exp. Fluids* **29**, 275-290.

Ahlborn, B., Harper, D. G., Blake, R. W., Ahlborn, D. and Cam, M. (1991). Fish without footprints. *J. Theor. Biol.* **148**, 521-533.

Akhtar, I. and Mittal, R. (2005). A biologically inspired computational study of flow past tandem flapping foils. *35th AIAA Fluid Dynamics Conf. Exhib.* Toronto, ON. AIAA 2005-4760.

Bainbridge, R. (1963). Caudal fin and body movements in the propulsion of some fish. *J. Exp. Biol.* **40**, 23-56.

Barnard, R. H. and Philpott, D. R. (1995). *Aircraft Flight*. London: Longman Group.

Barrett, D., Triantafyllou, M. S., Yue, D. K. P., Grosenbaugh, M. A. and Wolfgang, M. J. (1999). Drag reduction in fish-like locomotion. *J. Fluid Mech.* **392**, 183-212.

Batchelor, G. K. (1973). *An Introduction to Fluid Dynamics*. Cambridge: Cambridge University Press.

Breder, C. M. (1926). The locomotion of fishes. *Zoologica* **4**, 159-297.

Buchholz, J. and Smits, A. J. (2006). On the evolution of the wake structure produced by a low aspect ratio pitching panel. *J. Fluid Mech.* **546**, 433-443.

Carling, J., Williams, T. L. and Bowtell, G. (1998). Self-propelled anguilliform swimming: Simultaneous solution of the two-dimensional Navier–Stokes equations and Newton's laws of motion. *J. Exp. Biol.* **201**, 3143-3166.

Dabiri, J. O. (2005). On the estimation of swimming and flying forces from wake measurements. *J. Exp. Biol.* **208**, 3519-3532.

Dong, H., Mittal, R., Bozkurttas, M. and Najjar, F. (2005). Wake structure and performance of fine aspect ratio flapping foils. *43rd AIAA Aerosp. Sci. Meet. Exhib.* Reno, NV. AIAA 2005-0081.

Drucker, E. G. and Lauder, G. V. (1999). Locomotor forces on a swimming fish: three-dimensional vortex wake dynamics quantified using digital particle image velocimetry. *J. Exp. Biol.* **202**, 2393-2412.

Drucker, E. G. and Lauder, G. V. (2000). A hydrodynamic analysis of fish swimming speed: wake structure and locomotor force in slow and fast labriform swimmers. *J. Exp. Biol.* **203**, 2379-2393.

Drucker, E. G. and Lauder, G. V. (2001). Locomotor function of the dorsal fin in teleost fishes: experimental analysis of wake forces in sunfish. *J. Exp. Biol.* **204**, 2943-2958.

Drucker, E. G. and Lauder, G. V. (2005). Locomotor function of the dorsal fin in rainbow trout: kinematic patterns and hydrodynamic forces. *J. Exp. Biol.* **208**, 4479-4494.

Faber, T. E. (1995). *Fluid Dynamics for Physicists*. Cambridge: Cambridge University Press.

Ferry, L. A. and Lauder, G. V. (1996). Heterocercal tail function in leopard sharks: a three-dimensional kinematic analysis of two models. *J. Exp. Biol.* **199**, 2253-2268.

Gaydon, M., Raffel, M., Willert, C. E., Rosengarten, M. and Kompenhans, J. (1997). Hybrid stereoscopic particle image velocimetry. *Exp. Fluids* **23**, 331-334.

Gibb, A. C., Dickson, K. A. and Lauder, G. V. (1999). Tail kinematics of the chub mackerel *Scomber japonicus*: Testing the homocercal tail model of fish propulsion. *J. Exp. Biol.* **202**, 2433-2447.

Gonzalez, R. C., Woods, R. E. and Eddins, S. L. (2003). *Digital Image Processing using MATLAB*. Upper Saddle River, NJ: Pearson Education.

Gopalkrishnan, R., Triantafyllou, M. S., Triantafyllou, G. S. and Barrett, D. (1994). Active vorticity control in a shear flow using a flapping foil. *J. Fluid Mech.* **274**, 1-21.

Haller, G. (2005). An objective definition of a vortex. *J. Fluid Mech.* **525**, 1-26.

Hart, D. P. (2000). PIV error correction. *Exp. Fluids* **29**, 13-22.

Hartley, R. and Zissermann, A. (2000). *Multiple View Geometry in Computer Vision*. Cambridge: Cambridge University Press.

He, P. and Wardle, C. S. (1986). Tilting behavior of the Atlantic mackerel, *Scomber scombrus*, at low swimming speeds. *J. Fish Biol.* **29**, 223-232.

Helfman, G. S., Collette, B. B. and Facey, D. E. (1997). *The Diversity of Fishes*. London: Blackwell Science.

Jenkins, R. E. and Burkhead, N. M. (1994). *Freshwater Fishes of Virginia*. Bethesda, MD: American Fisheries Society.

Lauder, G. V. (2000). Function of the caudal fin during locomotion in fishes: kinematics, flow visualization, and evolutionary patterns. *Am. Zool.* **40**, 101-122.

Lauder, G. V. and Drucker, E. G. (2004). Morphology and experimental hydrodynamics of fish fin control surfaces. *IEEE J. Oceanic Eng.* **29**, 556-571.

Lauder, G. V. and Tytell, E. D. (2006). Hydrodynamics of undulatory propulsion. In *Fish Biomechanics* (ed. R. E. Shadwick and G. V. Lauder), pp. 425-468. San Diego: Academic Press.

Lauder, G. V., Nauen, J. C. and Drucker, E. G. (2002). Experimental hydrodynamics and evolution: Function of median fins in ray-finned fishes. *Integr. Comp. Biol.* **42**, 1009-1017.

Liao, J. and Lauder, G. V. (2000). Function of the heterocercal tail in white sturgeon: flow visualization during steady swimming and vertical maneuvering. *J. Exp. Biol.* **203**, 3585-3594.

Lighthill, J. (1960). Note on the swimming of slender fish. *J. Fluid Mech.* **9**, 305-317.

Lighthill, J. (1970). Aquatic animal propulsion of high hydromechanical efficiency. *J. Fluid Mech.* **44**, 265-301.
Lighthill, J. (1971). Large-amplitude elongated-body theory of fish locomotion. *Proc. R. Soc. Lond. B* **179**, 125-138.
Lindsey, C. C. (1978). Form, function, and locomotory habits in fish. In *Fish Physiology.* Vol. VII, *Locomotion* (ed. W. S. Hoar and D. J. Randall), pp. 1-100. New York: Academic Press.
Milliken, G. A. and Johnson, D. E. (1992). *Analysis of Messy Data,* Vol. 1, *Designed Experiments*. London: Chapman & Hall.
Müller, U. K., van den Heuvel, B.-L. E., Stamhuis, E. J. and Videler, J. J. (1997). Fish foot prints: morphology and energetics of the wake behind a continuously swimming mullet (*Chelon labrosus* Risso). *J. Exp. Biol.* **200**, 2893-2906.
Müller, U. K., Smit, J., Stamhuis, E. J. and Videler, J. J. (2001). How the body contributes to the wake in undulatory fish swimming: flow fields of a swimming eel (*Anguilla anguilla*). *J. Exp. Biol.* **204**, 2751-2762.
Nauen, J. C. and Lauder, G. V. (2002a). Hydrodynamics of caudal fin locomotion by chub mackerel, *Scomber japonicus* (Scombridae). *J. Exp. Biol.* **205**, 1709-1724.
Nauen, J. C. and Lauder, G. V. (2002b). Quantification of the wake of rainbow trout (*Oncorhynchus mykiss*) using three-dimensional stereoscopic digital particle image velocimetry. *J. Exp. Biol.* **205**, 3271-3279.
Nogueira, J., Lecuona, A. and Rodríguez, P. A. (1997). Data validation, false vectors correction and derived magnitudes calculation on PIV data. *Meas. Sci. Technol.* **8**, 1493-1501.
Pereira, F. and Gharib, M. (2002). Defocusing digital particle image velocimetry and the three-dimensional characterization of two-phase flows. *Meas. Sci. Technol.* **13**, 683-694.
Prasad, A. K. (2000). Stereoscopic particle image velocimetry. *Exp. Fluids* **29**, 107-115.
Press, W. H., Teukolsky, S. A., Vetterling, W. T. and Flannery, B. P. (1992). *Numerical Recipes in C*. Cambridge: Cambridge University Press.
Saffman, P. G. (1992). *Vortex Dynamics*. Cambridge: Cambridge University Press.
Schultz, W. W. and Webb, P. W. (2002). Power requirements of swimming: do new methods resolve old questions? *Integr. Comp. Biol.* **42**, 1018-1025.
Spedding, G. R., Rosen, M. and Hedenstrom, A. (2003). A family of vortex wakes generated by a thrush nightingale in free flight in a wind tunnel over its entire natural range of flight speeds. *J. Exp. Biol.* **206**, 2313-2344.
Standen, E. M. and Lauder, G. V. (2005). Dorsal and anal fin function in bluegill sunfish (*Lepomis macrochirus*): three-dimensional kinematics during propulsion and maneuvering. *J. Exp. Biol.* **208**, 2753-2763.
Taylor, G. I. (1952). Analysis of the swimming of long and narrow animals. *Proc. R. Soc. Lond. A* **214**, 158-183.
Tennekes, H. and Lumley, J. L. (1972). *A First Course in Turbulence*. Cambridge, MA: MIT Press.
Tytell, E. D. (2004). The hydrodynamics of eel swimming. II. Effect of swimming speed. *J. Exp. Biol.* **207**, 3265-3279.
Tytell, E. D. and Ellington, C. P. (2003). How to perform measurements in a hovering animal's wake: physical modelling of the vortex wake of the hawkmoth *Manduca sexta*. *Philos. Trans. R. Soc. Lond. B* **358**, 1559-1566.
Tytell, E. D. and Lauder, G. V. (2004). The hydrodynamics of eel swimming. I. Wake structure. *J. Exp. Biol.* **207**, 1825-1841.
Vollmers, H. (2001). Detection of vortices and quantitative evaluation of their main parameters from experimental velocity data. *Meas. Sci. Technol.* **12**, 1199-1207.
von Ellenrieder, K. D., Parker, K. and Soria, J. (2003). Flow structures behind a heaving and pitching finite-span wing. *J. Fluid Mech.* **490**, 129-138.
Walker, J. A. (1998). Estimating velocities and accelerations of animal locomotion: A simulation experiment comparing numerical differentiation algorithms. *J. Exp. Biol.* **201**, 981-995.
Warrick, D. R., Tobalske, B. W. and Powers, D. R. (2005). Aerodynamics of the hovering hummingbird. *Nature* **435**, 1094-1097.
Webb, P. W. (1975). Hydrodynamics and energetics of fish propulsion. *Bull. Fish. Res. Board Can.* **190**, 1-159.
Weihs, D. (1972). A hydrodynamical analysis of fish turning manoevers. *Proc. R. Soc. Lond. B* **182**, 59-72.
Wieneke, B. (2005). Stereo-PIV using self-calibration on particle images. *Exp. Fluids* **39**, 267-280.
Wilga, C. D. and Lauder, G. V. (2004). Hydrodynamic function of the shark's tail. *Nature* **430**, 850.
Willert, C. E. (1997). Stereoscopic digital particle image velocimetry for application in wind tunnel flows. *Meas. Sci. Technol.* **8**, 1465-1479.
Willert, C. E. and Gharib, M. (1991). Digital particle image velocimetry. *Exp. Fluids* **10**, 181-193.
Wolfgang, M. J., Anderson, J. M., Grosenbaugh, M. A., Yue, D. K. P. and Triantafyllou, M. S. (1999). Near-body flow dynamics in swimming fish. *J. Exp. Biol.* **202**, 2303-2327.
Wu, T. Y. (1971). Hydromechanics of swimming propulsion. Part 1. Swimming of a two-dimensional flexible plate at variable forward speeds in an inviscid fluid. *J. Fluid Mech.* **46**, 337-355.
Zhu, Q., Wolfgang, M. J., Yue, D. K. P. and Triantafyllou, M. S. (2002). Three-dimensional flow structures and vorticity control in fish-like swimming. *J. Fluid Mech.* **468**, 1-28.